LIFE SCIENCES

Sequential introgression of a carotenoid processing gene underlies sexual ornament diversity in a genus of manakins

Haw Chuan Lim[1,2]*†, Kevin F. P. Bennett[3,4]*†‡, Nicholas M. Justyn[5]§, Matthew J. Powers[5]¶, Kira M. Long[6]#, Sarah E. Kingston[7], Willow R. Lindsay[8], James B. Pease[9], Matthew J. Fuxjager[10], Peri E. Bolton[11,4]**, Christopher N. Balakrishnan[11,12], Lainy B. Day[8], Thomas J. Parsons[4], Jeffrey D. Brawn[13], Geoffrey E. Hill[5], Michael J. Braun[3,4]***

In a hybrid zone between two tropical lekking birds, yellow male plumage of one species has introgressed asymmetrically replacing white plumage of another via sexual selection. Here, we present a detailed analysis of the plumage trait to uncover its physical and genetic bases and trace its evolutionary history. We determine that the carotenoid lutein underlies the yellow phenotype and describe microstructural feather features likely to enhance color appearance. These same features reduce predicted water shedding capacity of feathers, a potential liability in the tropics. Through genome-scale DNA sequencing of hybrids and each species in the genus, we identify *BCO2* as the major gene responsible for the color polymorphism. The *BCO2* gene tree and genome-wide allele frequency patterns suggest that carotenoid-pigmented collars initially arose in a third species and reached the hybrid zone through historical gene flow. Complex interplay between sexual selection and hybridization has thus shaped phenotypes of these species, where conspicuous sexual traits are key to male reproductive success.

INTRODUCTION

Sexual selection has produced many remarkable physical and behavioral traits in animals (*1*). More broadly, sexual selection shapes biodiversity by promoting speciation, driving rapid diversification of extravagant phenotypes, and accelerating molecular evolution (*2*, *3*). Gaining insight into the evolution of sexually selected traits including ornamentation and other reproductive signals will be facilitated by understanding their genetic architecture. Whether a trait depends on few or many genes and the degree to which the underlying genes are involved in other traits or metabolic pathways have important implications for the trait's evolvability. While genes underlying most display traits remain unknown (*4*), rapid advances in genomics are creating unique opportunities to study sexual selection and reveal how it can work in concert—or at times, in conflict—with natural selection to produce the diversity we see in nature (*5*).

Parallel advances in speciation research are revealing the prevalence of hybridization and introgression in shaping the evolution of organisms (*6*). Introgression can enlarge the pool of genetic variation available to a species and assemble existing variants in unique combinations, which in turn become the raw materials that fuel further evolution and diversification (*7*). In addition, genetic elements underlying particular advantageous traits can sometimes introgress across species boundaries despite processes that purge foreign alleles in the genome (*8*). Although these topics have received increased attention in the genomics era, important work remains to establish the frequency of introgressive hybridization and its role in driving phenotypic changes, adaptive radiation, diversification, and even reticulate evolution (*9*). Some of the pertinent challenges include identifying introgressed traits that are under positive selection, measuring their fitness effects, determining their genetic architecture, and deciphering the interplay between positive and negative selection, which can limit the spread or persistence of introgressed elements in new environments or genomic backgrounds.

To date, most research on introgressive hybridization has investigated traits whose introgression was driven by natural selection [e.g., (*10*–*12*)], with fewer studies focusing on traits involved in mate preference or sexual selection [but see (*13*–*16*)]. One possible explanation for the apparent paucity of systems demonstrating such introgression is that sexual selection tends to be associated with accelerated phenotypic evolution and increased discrimination among diverging species on the basis of reproductive traits (*17*, *18*). Cases where introgression of sexually selected traits has been identified deserve careful study, both because their prevalence may be underappreciated and because

[1]Department of Biology, George Mason University, Fairfax, VA 22030, USA. [2]National Zoo and Conservation Biology Institute, Smithsonian Institution, Washington, DC 20013, USA. [3]Department of Biology and Biological Sciences Graduate Program, University of Maryland, College Park, MD 20742, USA. [4]Department of Vertebrate Zoology, National Museum of Natural History, Smithsonian Institution, Washington, DC 20013, USA. [5]Department of Biological Sciences, Auburn University, Auburn, AL 36830, USA. [6]Program in Ecology Evolution and Conservation Biology, University of Illinois Urbana-Champaign, Urbana, IL 61801, USA. [7]Sea Education Association, Woods Hole, MA 02543, USA. [8]Department of Biology and Interdisciplinary Neuroscience Minor, University of Mississippi, University, MS 38677, USA. [9]Department of Biology, Wake Forest University, Winston-Salem, NC 27109, USA. [10]Department of Ecology Evolution and Organismal Biology, Brown University, Providence, RI 02912, USA. [11]Department of Biology, East Carolina University, Greenville, NC 27858, USA. [12]Division of Environmental Biology, National Science Foundation, Alexandria, VA 22314, USA. [13]Department of Natural Resources and Environmental Sciences, University of Illinois, Urbana, IL 61801, USA.
*Corresponding author. Email: hlim22@gmu.edu (H.C.L.); bennettkf@si.edu (K.F.P.B.); braunm@si.edu (M.J.B.)
†These authors contributed equally to this work.
‡Present address: Department of Biology, Pennsylvania State University, State College, PA 16801, USA.
§Present address: Department of Biosciences, Swansea University, Swansea, SA2 8PP, UK.
¶Present address: Department of Integrative Biology, Oregon State University, Corvallis, OR, 97333, USA.
#Present address: Center for Conservation Genomics, Smithsonian National Zoo and Conservation Biology Institute, Washington, DC, 20008, USA.
**Present address: Department of Evolution, Ecology, and Organismal Biology, The Ohio State University, Columbus, OH 43210, USA.

they provide special opportunities to explore mechanisms of sexual selection, such as perceptual bias (*19*) or honest signaling (*20*).

The manakins (family Pipridae) are a group of birds in which males are under strong sexual selection. Manakins exhibit lek mating systems, including colorful male plumage and elaborate mating displays (*21*). They also display interesting hybridization dynamics: There are at least nine intergeneric crosses known in manakins, supporting early observations of increased rates of intergeneric hybridization in avian clades with high sexual dimorphism (*22*). Manakins also display interspecific hybrid zones (*13*, *23*–*25*) and one instance of apparent hybrid speciation (*24*), which has rarely been documented in birds. Among manakins, the species in the genus *Manacus* perform the most acrobatic courtship display (see movie S1) (*26*). The four species and several subspecies of *Manacus* replace each other geographically in humid lowland forests throughout the Neotropics, and hybrid zones occur in three areas where their ranges abut (Fig. 1A). Males differ conspicuously in the colors of their collar and belly plumage, which include bright whites, vibrant yellows, saturated oranges, olive-greens, and grays (Fig. 1B), and plumage coloration has been shown to correlate with male mating success (*27*, *28*).

Previous studies demonstrated a notable asymmetric introgression of male secondary sexual traits between two *Manacus* species—*M. candei* (white-collared manakin) and *M. vitellinus* (golden-collared manakin)—in northwestern Panama (*13*, *23*, *29*). In this region, the yellow collar plumage of male golden-collared manakins has introgressed beyond the genomic center of a hybrid zone between the species, producing hybrid populations that look like golden-collared manakins, but have genomic backgrounds of white-collared manakins (Fig. 1C). The spread of yellow collars into *M. candei* has not extended across the entirety of its range but has stabilized at the Río Changuinola, a river roughly 50 km from the center of the hybrid zone (*23*, *29*). Other secondary sexual traits of male golden-collared manakins, such as their olive-green belly plumage, narrow hindneck collar, aggressive behavior on leks, and at least one dance maneuver, have also introgressed asymmetrically but not to the extent of golden collars (*13*, *23*, *29*–*31*). Introgression of these traits appears to be driven by female mate choice (*28*) and male-male competition (*30*), but the failure of these traits to sweep to fixation in *M. candei* populations suggests that countervailing forces are at play (*32*).

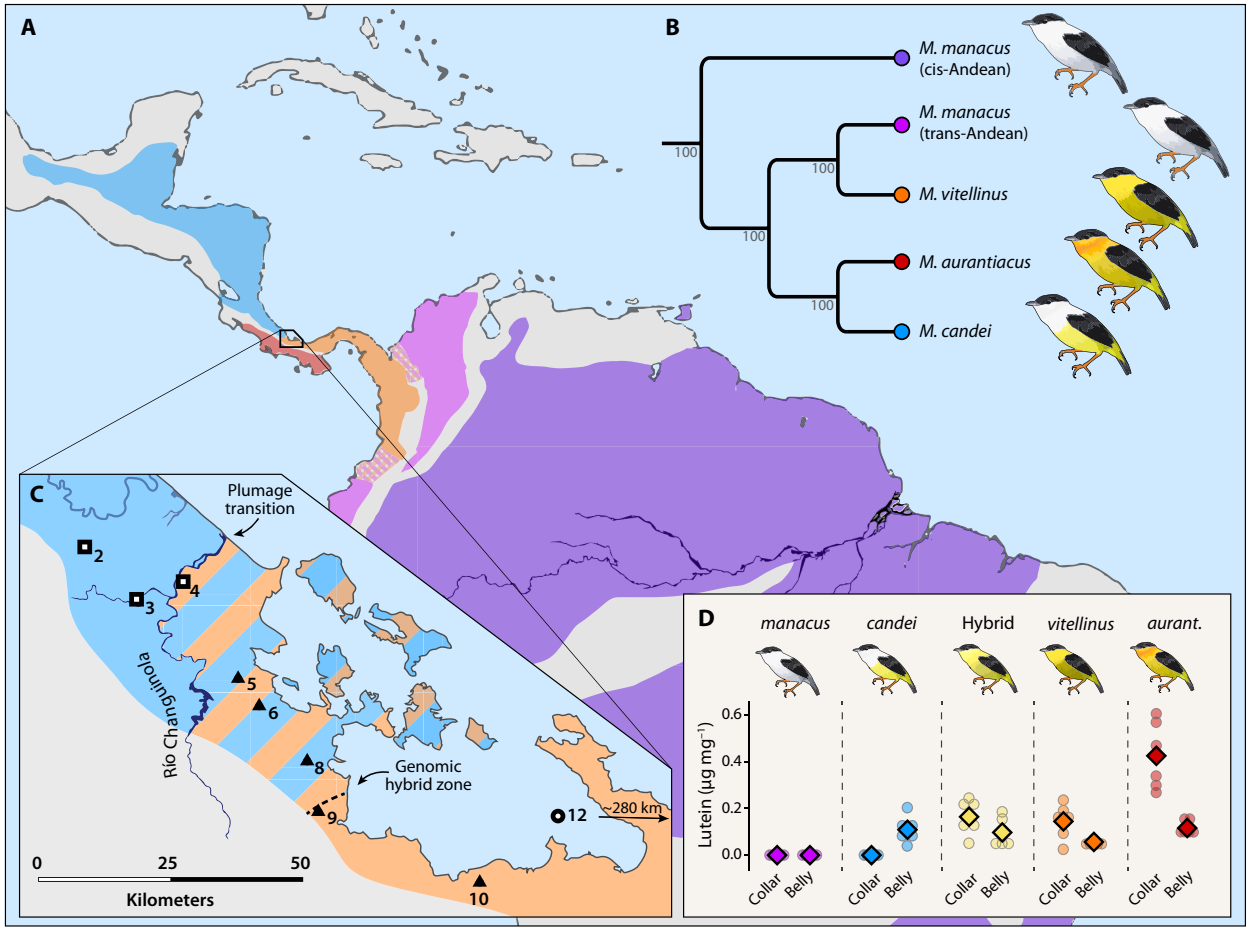

Fig. 1. Overview of *Manacus* system. (**A**) Distribution of major *Manacus* lineages. Cross-hatched regions are hybrid zones between *M. vitellinus* and *M. manacus* (*119*). (**B**) The species tree of *Manacus* with maximum likelihood bootstrap support values shown (*120*). (**C**) Hybrid zone between *M. vitellinus* (orange region) and *M. candei* (blue region), with plumage introgression shown in orange and blue stripes. Sampling sites for populations used in whole-genome resequencing (circles), RADseq (triangles), or both methods (squares). Site 12 is located at Gamboa in central Panama. (**D**) Lutein concentrations of *Manacus* collar and belly feathers. Circles indicate replicate individuals, and diamonds indicate means.

Because of the unusual introgression dynamics present in this system and its occurrence in a group marked by intense sexual selection, we sought to understand the evolutionary processes that gave rise to the diversity of plumage color in *Manacus* manakins. In this study, we first characterized the biochemical and microstructural contributors to color variation in male collar and belly plumage and then used whole-genome resequencing data to identify a major gene involved in the yellow/white collar polymorphism and trace its evolutionary history in the genus.

RESULTS

Feather pigmentation

Using quantitative high-performance liquid chromatography (HPLC) with carotenoid standards, we found only a single carotenoid pigment—lutein—in male collar and belly feathers of *Manacus* species or hybrids (fig. S1). The concentration of lutein largely determined the coloration of collar plumage (Figs. 1D and 2A and table S2A). White collar feathers of *M. manacus* and *candei* had no detectable lutein, while yellow collar feathers of *M. vitellinus* and birds in the plumage introgression region (hereafter, "hybrids") had intermediate lutein levels. The orange collar feathers of *Manacus aurantiacus* had lutein concentrations that were significantly higher than each of the other taxa (Table 1). In belly feathers, *M. manacus* had no lutein. Among the taxa with lutein-pigmented bellies, the only significant difference was between *M. aurantiacus*, which had the highest concentration, and *M. vitellinus*, which had the lowest (Table 1 and table S2A).

We modeled the effect of lutein concentrations on colorimetric variables calculated from reflectance spectra using pavo (Fig. 2, B and D) (*33*). For collar feathers, these analyses showed that lutein concentration was significantly and positively correlated with yellow saturation, carotenoid (i.e., all yellow-to-red wavelengths) chroma, and hue (Fig. 2, E and F, and Table 1). Lutein concentration did not significantly predict collar feather brightness and was negatively correlated with ultraviolet (UV) wavelength saturation (fig. S2 and Table 1). These relationships were unchanged when belly feathers (which contained visible melanosomes) were included in the analysis along with a melanization term (table S2D).

Using light microscopy, we qualitatively characterized the visible melanization patterns of *Manacus* collar and belly feathers. Typical feathers are bipinnate structures composed of a central rachis extending from the skin, barbs extending from the rachis, and barbules extending from the barbs (Fig. 2A). We found no visible evidence of melanin in collar feathers of any *Manacus* species or hybrids (Fig. 2A). Yellow belly feathers of *M. candei* also contained no visible melanin (Fig. 2C). Belly feathers of trans-Andean *M. manacus* (ssp. *abditivus*), which appear gray to the naked eye, had white barbs and barbules, with black stripes running the full length of the barbules (Fig. 2C). We presume these stripes to be clusters of melanosomes. Belly feathers of *M. vitellinus*, *aurantiacus*, and *candei* x *vitellinus* hybrids contained varying amounts of lutein in barbs and melanosomes in barbules, producing dark olive-green shades in *vitellinus*, dull yellow to olive in *aurantiacus*, and yellow to dark olive-green in hybrids (Fig. 2C). Belly feathers of *M. vitellinus* generally had heavily melanized barbules. *M. aurantiacus* had some melanized barbules in the center of belly feathers, but the barbules became small, lost melanization, and were usually orange toward the distal end. In hybrids, the presence of melanosomes in barbules was sporadic, making belly feathers olive-green in some individuals and yellow in others. Thus, whether lutein-pigmented *Manacus* belly feathers appeared olive-green or yellow is a function of melanin deposition in the barbules. The variable degree of melanosome deposition in hybrids reflects the fact that the geographic extent of olive-green belly color introgression trailed that of yellow collar coloration at the time the specimens were collected in 1991 (*23*); however, belly color has introgressed further in the past 30 years (*29*).

Feather microstructure

Aspects of feather microstructure differed by species, plumage patch, and color. Carotenoid-pigmented collar feathers of *M. vitellinus* and *aurantiacus* had significantly wider barbs than white collar feathers of *M. manacus* and *candei* (Table 2, Fig. 2A, and fig. S3). Hybrids' collar feathers had barbs of intermediate width, but they were significantly different only from *aurantiacus*. Barbule morphology also varied among the taxa. *M. manacus* and *candei* collar feathers had barbules typical of avian contour feathers, while *vitellinus* and *aurantiacus* collar feathers lacked barbules on roughly the distal third of the feather (Fig. 2A). Hybrids had barbules that appeared smaller than those of *M. manacus* or *candei* but not as greatly reduced as those of *vitellinus* or *aurantiacus* (Fig. 2A).

To explore the effect of barb width on collar color, we modeled correlations between barb width and colorimetric variables from reflectance spectra. Because barb width was positively correlated with lutein concentration ($P = 0.0071$), we included lutein concentration as a covariate in each model. Even controlling for lutein, barb width was significantly correlated with feather brightness and hue in collar feathers, with wider barbs showing decreased brightness and more red-shifted hues (Table 2).

To further explore the effect of feather microstructure on color, we compared yellow belly feathers of *M. candei*, which have fully formed barbules (Fig. 2C), to yellow collar feathers of *vitellinus* and hybrids, which have reduced or missing barbules (Fig. 2A). There was no significant difference in lutein concentration among these three (Table 1 and table S3A), but both *M. vitellinus* and hybrid collar feathers had significantly higher yellow saturation, higher carotenoid chroma, and lower UV saturation—essentially, purer and more saturated yellow coloration—than *candei* belly feathers (table S3).

Microstructural changes can affect the physical properties of feathers in addition to their color. A property of avian contour feathers that is especially important in the humid tropical forests where these manakins live is their ability to shed water. To investigate potential fitness consequences of the observed differences in feather microstructure, we estimated water repellency of *Manacus* collar feathers using a model from textiles science that has frequently been used in ornithology (*34*, *35*). When applied to feathers, this model estimates the beading of water on feather vanes using a simple structural index dependent only on measurements of barb width and barb spacing. Our water repellency estimates indicated that *M. vitellinus* and *M. aurantiacus*, the two species with carotenoid-pigmented collar feathers and accompanying microstructural modifications, had the poorest ability to shed water when compared to the species with white collars (Fig. 2G and fig. S3C), while hybrids showed intermediate water shedding ability. Differences in barb width appeared to drive these differences in estimated water repellency among *Manacus* collar feathers (fig. S3A) because barb spacing was similar among taxa, with a statistically significant difference only between white-collared *M. candei* and *M. manacus* (fig. S3B and table S4).

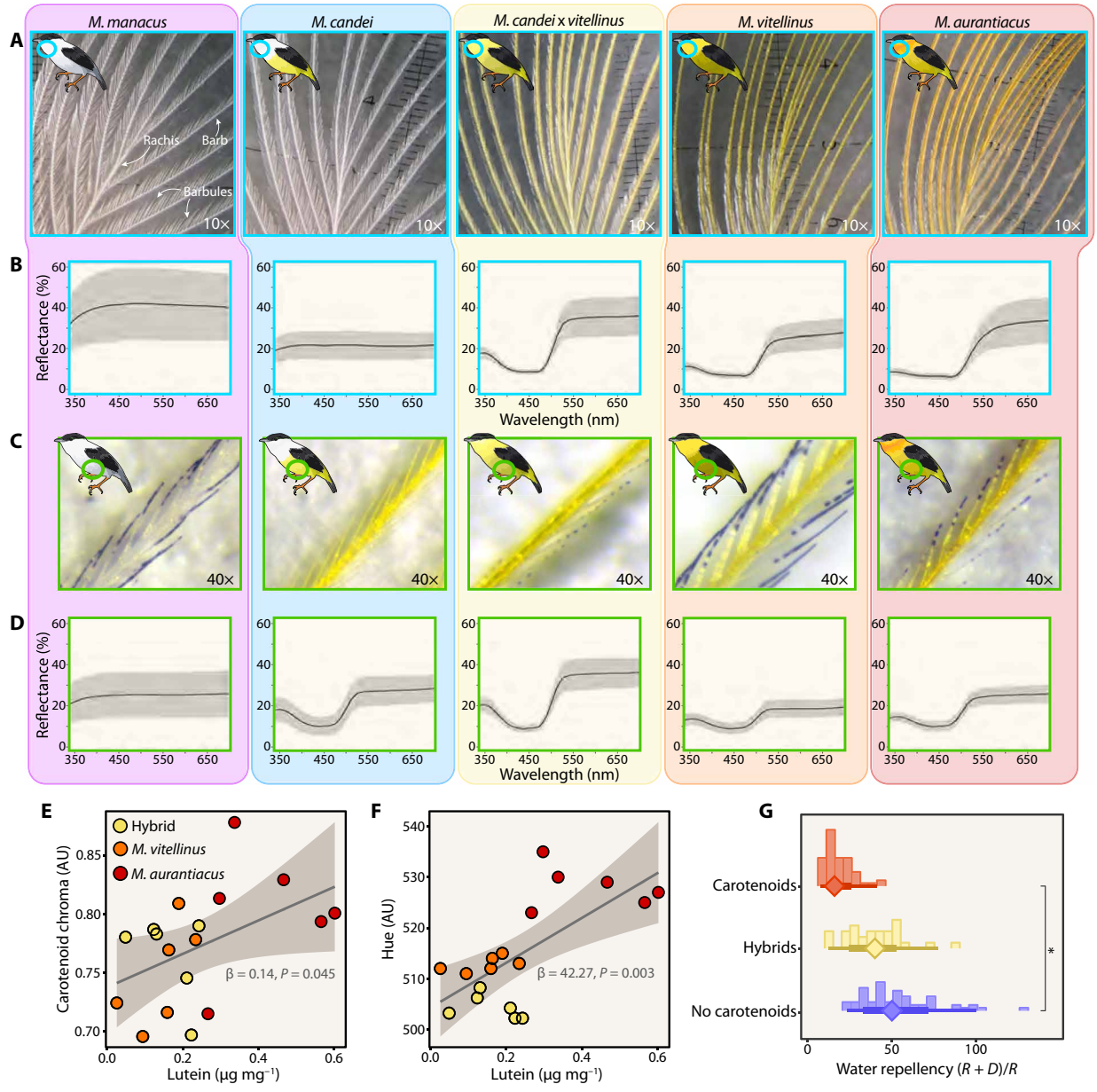

Fig. 2. Feather color, microstructure, and water repellency differences among *Manacus* species. (**A** and **C**) Microscope images of collar (A) and belly (C) feathers of *Manacus* species showing variation in color and microstructural morphology of barbs and barbules. *M. vitellinus*, *M. aurantiacus*, and, to a lesser extent, hybrids display reduced number and size of barbules toward the distal ends of the collar feather barbs. (**B** and **D**) Reflectance spectra of collar (B) and belly (D) plumage of *Manacus* species. (**E** and **F**) The modeled effect of lutein concentration in collar feathers on yellow-red wavelength chroma (E) and hue (F). AU, arbitrary units. (**G**) Predicted water repellency of *Manacus* collar feathers. "Carotenoids" refers to *M. aurantiacus* and *M. vitellinus*, hybrids refers to *M. vitellinus* x *M. candei* hybrids, and "no carotenoids" refers to *M. candei* and *M. manacus*. The asterisk indicates a statistically significant ($\alpha < 0.05$) difference between groups.

Genetic basis of plumage color

To investigate the genetic basis of traits that have introgressed asymmetrically across the *vitellinus-candei* hybrid zone, we resequenced whole genomes of two parental *candei* and four parental *vitellinus* (sites 2 and 12, Fig. 1C), as well as 10 males from each of two focal populations separated by less than 8 km across the Río Changuinola (sites 3 and 4, Fig. 1C). Genomes of these focal populations are predominantly derived from *candei* (*29*, *36*); but while males from site 3 have white collars, males from site 4 have yellow collars (*23*). The genomic similarity (figs. S4 and S5) and ongoing gene flow between these cross-river focal populations (tables S7 to S9 and figs. S6 to S8), the color difference between them, and the relatively deep divergence of the parental species (~0.97 million years; table S9) combine to create ideal conditions to isolate the genetic basis of collar coloration. Several other *M. vitellinus* traits (belly color, collar width, and aggression at leks) have introgressed to varying degrees (*13*, *23*, *29*, *30*) but were not fixed at site 4 on the east bank of the Río Changuinola when the samples sequenced here were collected. As a

Table 1. Feather lutein variation and effects on color in *Manacus*. Results from statistical models that contrast lutein concentration in collar feathers among species, contrast lutein concentration in belly feathers among species, and estimate the relationship between lutein concentration and reflectance measurements in pigmented collar feathers. Lutein concentration data for each species are in table S2A. Bolded values correspond to contrasts or variables where differences or effects are statistically significant at $P = 0.05$.

Lutein concentration - collar

Contrast	Estimate (β)	SE	df	*t*.ratio	*P* value	Lower CI	Upper CI
M. vitellinus - hybrid	−0.0281	0.0491	25	−0.572	0.9780	−0.172	0.116
M. vitellinus - *M. aurantiacus*	−0.2773	0.0491	25	−5.651	**0.0001**	**−0.421**	**−0.133**
M. vitellinus - *M. manacus*	0.3648	0.0491	25	7.434	**<0.0001**	**0.221**	**0.509**
M. vitellinus - *M. candei*	0.3648	0.0491	25	7.434	**<0.0001**	**0.221**	**0.509**
Hybrid - *M. aurantiacus*	−0.2493	0.0491	25	−5.080	**0.0003**	**−0.393**	**−0.105**
Hybrid - *M. manacus*	0.3928	0.0491	25	8.005	**<0.0001**	**0.249**	**0.537**
Hybrid - *M. candei*	0.3928	0.0491	25	8.005	**<0.0001**	**0.249**	**0.537**
M. aurantiacus - *M. manacus*	0.6421	0.0491	25	13.085	**<0.0001**	**0.498**	**0.786**
M. aurantiacus - *M. candei*	0.6421	0.0491	25	13.085	**<0.0001**	**0498**	**0.786**
M. manacus - *M. candei*	0.0000	0.0491	25	0.000	1.000	−0.144	0.144

Lutein concentration - belly

Contrast	Estimate (β)	SE	df	*t*.ratio	*P* value	Lower CI	Upper CI
M. vitellinus - hybrid	−0.0755	0.0354	25	−2137	0.2365	−0.1794	0.0283
M. vitellinus - *M. aurantiacus*	−0.1149	0.0354	25	−3.251	**0.0248**	**−0.2188**	**−0.0111**
M. vitellinus - *M. manacus*	0.2261	0.0354	25	6.394	**<0.0001**	**0.1222**	**0.3299**
M. vitellinus - *M. candei*	−0.0934	0.0354	25	−2.641	0.0929	−0.1972	0.0105
Hybrid - *M. aurantiacus*	−0.0394	0.0354	25	−1.114	0.7975	−0.1432	0.0644
Hybrid - *M. manacus*	0.3016	0.0354	25	8.531	**<0.0001**	**0.1978**	**0.4054**
Hybrid - *M. candei*	−0.0178	0.0354	25	−0.504	0.9862	−0.1217	0.0860
M. aurantiacus - *M. manacus*	0.3410	0.0354	25	9.645	**<0.0001**	**0.2372**	**0.4448**
M. aurantiacus - *M. candei*	0.0216	0.0354	25	0.610	0.9722	−0.0823	0.1254
M. manacus - *M. candei*	−0.3194	0.0354	25	−9.035	**<0.0001**	**−0.4232**	**−0.2156**

Effect of lutein concentration on pigmented collar feather colorimetric variables

Dependent variable	Estimate (β)	SE	*P* value	Lower CI	Upper CI
Yellow saturation*	0.07579	0.02559	**0.00919**	**0.02154**	**0.13**
UV saturation†	−0.09862	0.03237	**0.00769**	**−0.1672**	**−0.03**
Carotenoid chroma‡	0.14216	0.06521	**0.0446**	**0.003906**	**0.2804**
Mean brightness§	−2.794	6.877	0.69	−17.3735	11.785
Mid hue¶	42.273	12.102	**0.00301**	**16.618**	**67.9271**

*Pavo variable S1Yellow. †Pavo variable S1UV. ‡Pavo variable S9carotchroma. §Pavo variable b2meanbright. ¶Pavo variable H3huermid.

result, we expected the genomic signal of collar coloration to be strongest when comparing our focal sites.

We mapped the resequencing data to a reference genome for *M. vitellinus*, aligned reference scaffolds to chromosomes from another manakin assembly (*Chiroxiphia lanceolata*), and identified single-nucleotide polymorphisms (SNPs) that fit the allele frequency pattern expected for genomic regions responsible for introgressing *vitellinus* traits. Specifically, we filtered the data for strongly differentiated SNPs ("dSNPs") that were missing no more than 50% of genotypes in parental *candei* and *vitellinus* populations (sites 2 and 12, Fig. 1C), were fixed for different alleles between parental populations, had ≥80% *M. candei* allele frequency at site 3, where all males have white collars, and had ≥80% *M. vitellinus* allele frequency at site 4, where all males have yellow collars. There were 192 such dSNPs across the entire 1.1-Gb genome, 186 of which were clustered in a few regions on four putative chromosomes (2, 20, 24, and Z; Fig. 3A). No other chromosome had more than one dSNP (data S1). We further filtered dSNPs to consider only those fixed at either site 3 or 4. Of 53 such "fixed" dSNPs, 46 of them were in a haplotype block of 72 kb on chromosome 24 (Fig. 3, A and I). This block contains three genes, including Beta-Carotene Oxygenase 2 (*BCO2*), which encodes an enzyme that cleaves yellow carotenoids, including lutein, into colorless products (Fig. 3, I and J) (*37*). The two other genes in this block (Fig. 3J and fig. S28) were *TEX12*, which is involved in spermatogenesis (*38*), and *PTS*, which is involved in synthesis of an amino acid hydroxylase cofactor (*39*).

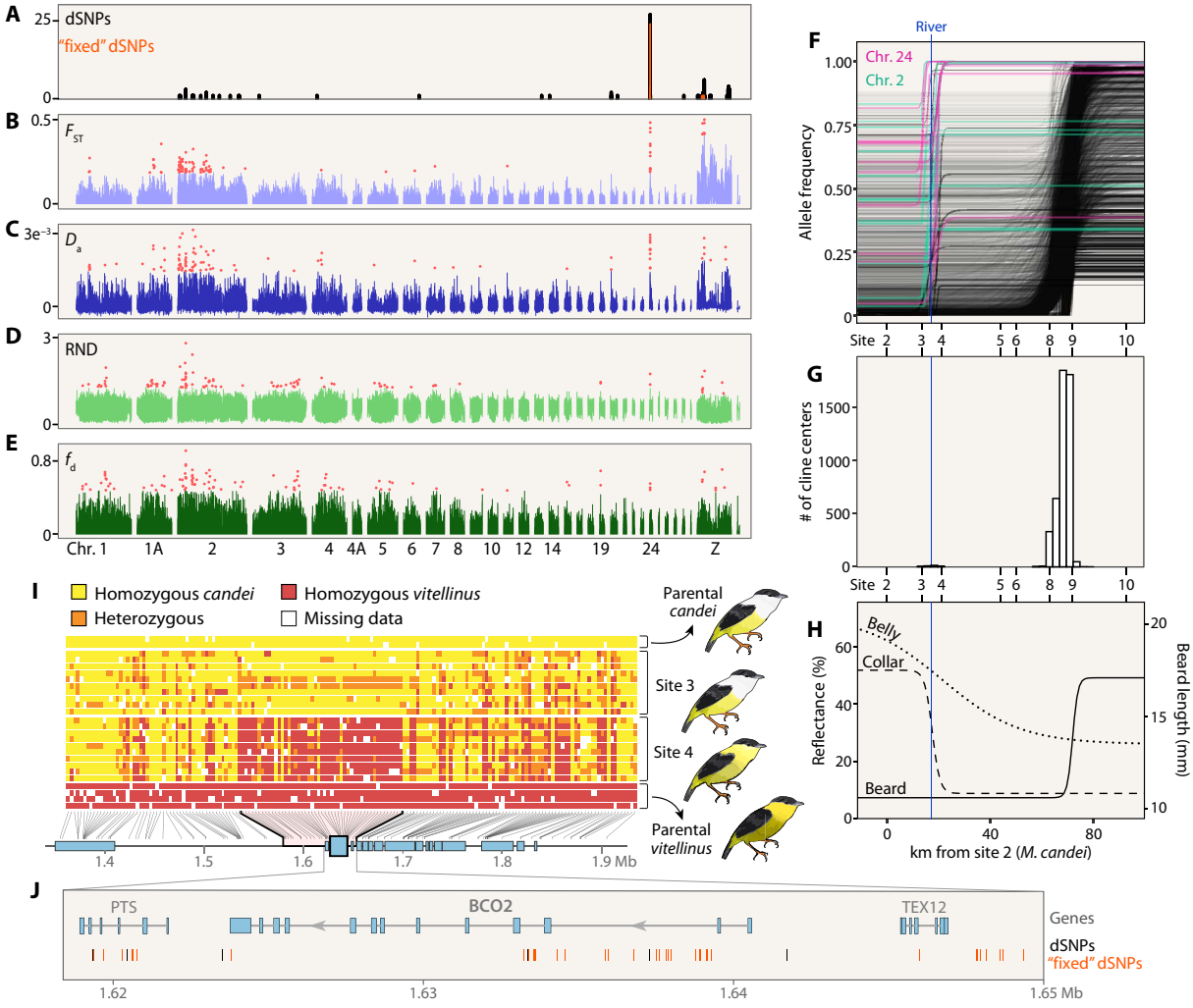

Fig. 3. Genomic evidence implicating *BCO2* in the collar color difference between *M. vitellinus* and *M. candei*. (**A**) Density of SNPs showing strong association with collar color in sites 3 and 4 (dSNPs) in 10-kb windows. Fixed dSNPs, overlaid in front, are a more strongly differentiated subset of dSNPs. (**B** to **E**) Differentiation and introgression metrics averaged in 10-kb windows across the genome. Autosomal and Z chromosome 99.9% outliers are indicated in red. Scans of 25- and 50-kb windows produced similar patterns (fig. S8). (B) and (C) Differentiation metrics F_{ST} and D_a, respectively, for sites 3 and 4. (D) and (E) Introgression metrics relative node depth (RND) and f_d, respectively. (**F** to **H**) Genetic and phenotypic clines across the hybrid zone from sites 2 to 10. (F) Clines for 4750 SNPs from RADseq data. Clines with centers displaced by more than 50 km from the main cluster of clines are highlighted in pink (chromosome 24), teal (chromosome 2), or black (other chromosomes). (G) Histogram of all SNP cline center locations. (H) Phenotypic clines in collar color (% reflectance at 490 nm), belly color (% reflectance at 665 nm), and beard length. (**I**) Individual genotypes for all SNPs fixed for different alleles between parental *M. vitellinus* (site 12) and *M. candei* (site 2) in the region of chromosome 24 around carotenoid metabolism gene *BCO2*. The bold black lines and pink shading indicate the inferred boundaries of the core block of DNA that has introgressed from *M. vitellinus* as far as site 4. (**J**) Locations of dSNPs (black tick marks) and fixed dSNPs (orange tick marks) around the *BCO2* gene. Exons are shown as blue boxes.

Table 2. Collar feather barb width variation and effects on color in *Manacus*. Results from statistical models that contrast barb width among species' collar feathers and estimate the relationship between barb width and reflectance measurements in pigmented collars, controlling for lutein concentration. Bolded values correspond to contrasts or variables where differences or effects are statistically significant at $P = 0.05$.

Barb width

Contrast	Estimate (β)	SE	df	*t*.ratio	*P* value	Lower CI	Upper CI
M. manacus - *M. candei*	−1.97085	2.974	25	−0.6627	0.962556	−10.7045	6.762774
M. manacus - hybrid	−6.1235	2.974	25	−2.0590	0.268657	−14.8571	2.610125
M. manacus - *M. vitellinus*	−14.6635	2.971	25	−4.9347	**<0.0001**	**−23.3918**	**−5.93523**
M. manacus - *M. aurantiacus*	−25.8807	2.974	25	−8.7021	**<0.0001**	**−34.6143**	**−17.1471**
M. candei - hybrid	−4.15265	2.974	25	−1.3963	0.635563	−12.8863	4.580973
M. candei - *M. vitellinus*	−12.6926	2.971	25	−4.2715	**0.002105**	**−21.4209**	**−3.96438**
M. candei - *M. aurantiacus*	−23.9098	2.974	25	−8.0394	**<0.0001**	**−32.6434**	**−15.1762**
Hybrid - *M. vitellinus*	−8.54	2.971	25	−2.8740	0.0573	−17.2683	0.188264
Hybrid - *M. aurantiacus*	−19.7572	2.974	25	−6.6431	**<0.0001**	**−28.4908**	**−11.0236**
M. vitellinus - *M. aurantiacus*	−11.2172	2.971	25	−3.7749	**0.007185**	**−19.9454**	**−2.48892**

Effect of barb width on pigmented collar feather colorimetric variables

Dependent variable	Estimate (β)	SE	*P* value	Lower CI	Upper CI
Yellow saturation*	1.91×10^{-4}	5.41×10^{-4}	0.7296	-9.63×10^{-4}	1.34×10^{-3}
UV saturation†	-6.39×10^{-4}	6.59×10^{-4}	0.3479	-2.04×10^{-3}	7.66×10^{-4}
Carotenoid chroma‡	-1.18×10^{-3}	1.38×10^{-3}	0.4084	-4.12×10^{-3}	1.77×10^{-2}
Mean brightness§	−0.2986	0.1272	**0.0331**	**−0.5698**	**−0.0274**
Mid hue¶	0.5448	0.2135	**0.0221**	**0.0898**	**0.9998**

*Pavo variable S1Yellow. †Pavo variable S1UV. ‡Pavo variable S9carotchroma. §Pavo variable b2meanbright. ¶Pavo variable H3huermid.

To test the geographic concordance of SNP markers with introgressed plumage traits, we examined a separate restriction site–associated DNA sequencing (RADseq) dataset from 152 individuals across the entire hybrid zone (Fig. 1C and table S14). From this genome-wide dataset, we retained 4750 high-quality SNPs showing clear clinal variation in allele frequency within the hybrid zone transect. Cline centers for the vast majority of these SNPs fell near site 9 (Fig. 3F), marking the major genomic transition from *M. vitellinus* to *M. candei*, in agreement with previous analyses (*23*, *36*). However, cline centers for 34 SNPs were located more than 50 km to the northwest (Fig. 3G), falling near the Río Changuinola and the limit of color introgression (Fig. 3H). Of these 34 SNPs with displaced cline centers, 10 are clustered in a genomic span of 768 kb on chromosome 24 surrounding the *BCO2* gene (Fig. 3F and data S2).

To further localize DNA blocks that have introgressed, we conducted sliding window scans of the resequencing data, calculating metrics of differentiation and introgression in non-overlapping 10-kb genomic windows (Fig. 3, B to E). The use of multiple summary statistics leverages different aspects of the data, and concordant signals among them increase the likelihood of detecting true positives (*40*, *41*). We therefore used F_{ST} and D_a (*42*) to gauge levels of genetic differentiation between focal sites 3 and 4, and we used f_d (*43*) and relative node depth (RND) (*44*) to infer introgression from parental *M. vitellinus* (site 12) into the yellow-collared hybrid population (site 4). We treated as outliers all 10-kb windows with extreme values for at least one statistic exceeding the 99.9th percentile (Fig. 3, B to E). These analyses revealed several genomic neighborhoods with high concentrations of strongly supported windows, each containing outliers for multiple statistics (fig. S9). These neighborhoods included regions in chromosomes 2 (690 kb) and 24 (140 kb around *BCO2*) and the Z sex chromosome (590 kb) (Fig. 3, B to E; figs. S10 to S33; and table S10; see Supplementary Text for details). In addition to carotenoid metabolism, genes adjacent to or within strongly supported genomic windows span a wide range of functions related to angiogenesis, feather/follicle development, solute transport, and spermatogenesis (table S11). Gene ontology–based analyses revealed pathways or molecular functions that were enriched with genes found within or around outlier genomic windows (tables S12 and S13). Among these pathways were several with

plausible connections to traits of interest, but none survived multiple testing correction. See Supplementary Text for further discussion.

BCO2 is the strongest candidate for a gene of major effect driving introgression of collar color in this system. The genomic region around *BCO2* contained multiple windowed outliers, displaced SNP clines, and numerous SNPs fixed for the *vitellinus* allele in site 4 and almost fixed (except for two heterozygous individuals) for the *candei* allele in site 3 (Fig. 3I). *BCO2* has been implicated in carotenoid color polymorphisms in a variety of organisms [e.g., (*45*–*47*)], including cases of interspecific introgression (*48*, *49*). Because BCO2 cleaves yellow carotenoids into colorless products when active (*37*), we expect the pigmented collar phenotypes of *Manacus* to be associated with reduced BCO2 activity in relevant tissues during feather growth, either due to reduced gene expression or inactivity of the enzyme (*48*, *50*–*52*). The amino acid sequences predicted by the white-collared and yellow-collared haplotypes are identical, and nucleotide substitutions were concentrated in introns and noncoding regions 5′ or 3′ of the gene (Fig. 3J). Thus, mutations that are functionally relevant to the yellow phenotype likely cause reduced gene expression in *M. vitellinus* either constitutively or in key tissues at crucial times for feather growth. Available RNA sequencing data showed that *BCO2* expression levels were higher in brain and lower in muscle tissues of *M. vitellinus* when compared to those of related species, suggesting that the gene is under tissue-specific regulation (fig. S34).

Our suite of analyses identified several other genes with plausible connections to introgressing traits across the hybrid zone. Of 192 dSNPs in the genome (data S1), 4 fell in a region on chromosome 20 between 25 and 114 kb upstream of Agouti Signaling Protein (*ASIP*), which encodes a polypeptide involved in regulating melanogenesis and commonly underlying melanin-based color variation [e.g., (*53*, *54*)]. Sliding windows (table S10) and dSNPs (data S1) both implicated Retinol Dehydrogenase 10 (*RDH10*) on chromosome 2. This gene has not previously been associated with color variation, but it encodes an enzyme involved in the linked metabolism of carotenoids and retinoids (*37*). A third region of interest, identified by dSNPs, sliding windows, and shifted RADseq clines, fell on chromosome 2 between the genes R-spondin 2 (*RSPO2*) and Eukaryotic Translation Initiation Factor 3 subunit E (*EIF3E*) (table S10 and data S1 and S2). *RSPO2* has the most obvious connection to plumage: It is a regulator of *Wnt* (*55*), which has been implicated in other instances of plumage patterning (*56*), and *RSPO2* controls major variation in domestic dog hair growth (*57*), which could indicate a connection to follicle development. For more discussion of introgressing genes, see Supplementary Text.

History of *BCO2* gene flow in *Manacus*

The two *Manacus* species with carotenoid-pigmented collars (*M. vitellinus* and *aurantiacus*) are not sister taxa (Fig. 1B), but both use lutein to produce their orange/yellow coloration (Fig. 2 and fig. S1). We wondered whether pigmented collars had a single origin in this genus or might have arisen independently. The two species are not now in contact, but their ranges come within ~25 km in central Panama (*58*, *59*), and hybridization could have occurred through long-distance dispersal or during past periods of contact. To test this question, we sequenced whole genomes of additional manakins representing the remaining major lineages of the genus (table S15). We constructed phylogenetic trees from a 48-kb region centered around *BCO2* and from "control" regions of 306 and 384 kb around two other genes also on chromosome 24 but with no known relationship to coloration (Fig. 4B). Topologies of the control gene trees (Fig. 4, D and E) matched the strongly supported species tree (Fig. 1B), with *M. aurantiacus* sister to *candei* and *vitellinus* sister to trans-Andean *manacus*. In the *BCO2* gene tree, however, *vitellinus* was sister to *aurantiacus*, and the *vitellinus-aurantiacus* clade was sister to *candei*, both with strong branch support (Fig. 4C). The fact that *vitellinus* moves from its position on the species tree to become sister to *aurantiacus* in the gene tree rather than the reverse indicates that the *BCO2* sequence now present in *vitellinus* originated in the *aurantiacus* genomic background (Fig. 4A).

Because discordance between gene trees and species trees can arise from several processes, we also looked for genome-wide evidence of introgression between *vitellinus* and *aurantiacus* using allele frequency patterns. We calculated f_d in 10-kb windows using trans-Andean *M. manacus*, *vitellinus*, *aurantiacus*, and cis-Andean *manacus* as test taxa and identified outliers exceeding the 99.9th percentile. A window 10 kb upstream of *BCO2* had the fifth highest f_d value of ~78,000 genome-wide windows (Fig. 4, F and G).

To localize the signal of introgression from *M. aurantiacus* to *vitellinus* at a finer scale, we repeated the f_d calculation in 2-kb windows across chromosome 24 (Fig. 4I). We also estimated local gene trees based on 100-bp non-overlapping windows and calculated the frequency of trees in 10- and 2-kb windows showing the topology expected under gene flow, with *M. aurantiacus* sister to *vitellinus* (Fig. 4, H and J). These two metrics—f_d and frequency of "gene flow" topologies—identified different stretches of DNA in the vicinity of *BCO2* as containing the strongest signals, with the highest f_d peak occurring just upstream of the gene and the highest proportion of gene flow trees occurring just downstream of the gene (Fig. 4, J and I). Together, these results all support directional gene flow from *M. aurantiacus* into *vitellinus* at *BCO2*, including a considerable introgression signal within the same block that has introgressed across the *M. vitellinus-candei* hybrid zone.

DISCUSSION

Feather color and microstructure

Through HPLC, spectrophotometry, and light microscopy, we found that color production in belly and collar feather patches among the major lineages of *Manacus* can be explained largely by the concentration of the carotenoid lutein, the presence or absence of melanin, and feather microstructure, including barb morphology and the presence or absence of barbules.

Differences in lutein concentrations of pigmented collar feathers affected saturation, chroma, and hue, as predicted by simulations of carotenoid absorbance (*60*). Orange feathers of *M. aurantiacus* contained more lutein than yellow feathers of *M. vitellinus* and *vitellinus* x *candei* hybrids. Yellow bellies of *M. candei* and some hybrids contained only lutein, while olive-green bellies of hybrids, *vitellinus*, and *aurantiacus* contained both lutein and melanized feather barbules. Gray bellies of *M. manacus* contained only melanin. Adding or reducing carotenoids in a plumage patch may be one of the simplest ways to create differences in color (*60*). On the basis of our light microscopy observations, we believe that adding melanized barbules could be another "simple" mechanism by which plumage color can be changed, although melanism is not associated with dichromatism as often as deposition of carotenoids (*61*).

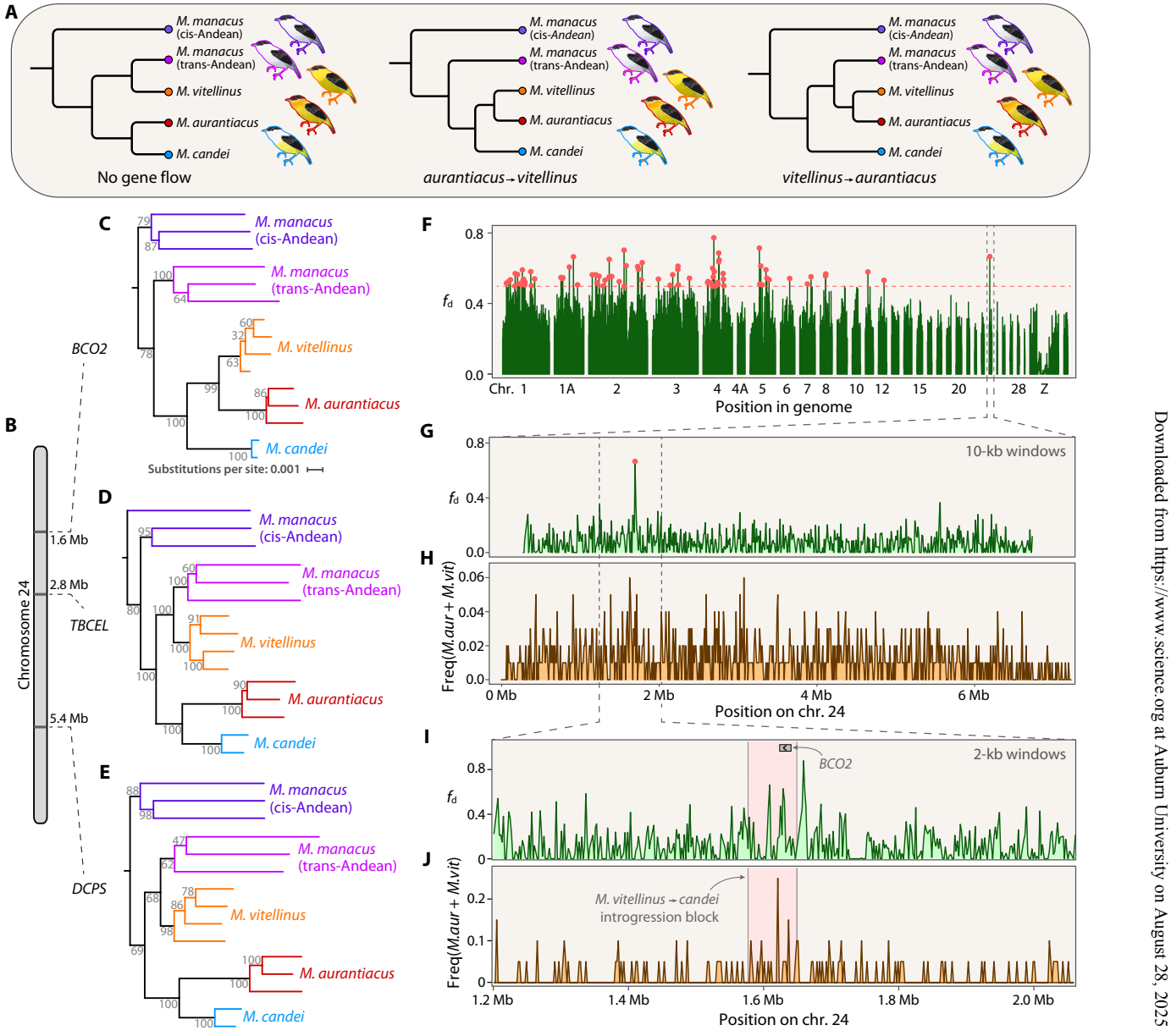

Fig. 4. Evidence for historical *BCO2* introgression between *M. aurantiacus* and *M. vitellinus*. (**A**) Gene trees expected under three different potential introgression scenarios. Lack of introgression results in a topology similar to the species tree. Directional introgression results in a discordant topology where the gene flow recipient shifts to the branch of the gene flow donor. (**B**) Locations of *BCO2* and two control genes (*TBCEL* and *DCPS*) on chromosome 24. (**C** to **E**) Gene trees generated using three regions on chromosome 24 for all major lineages in *Manacus*. Branch labels are maximum likelihood bootstrap support. (C) A 48-kb region including the gene *BCO2*, (D) a 384-kb region including the gene *TBCEL*, and (E) a 306-kb region including the gene *DCPS*. (**F** and **G**) Introgression metric f_d calculated between *M. aurantiacus* and *M. vitellinus* in 10-kb windows with 99.9% outliers in red. (F) The entire genome and (G) just chromosome 24. (**H**) Proportions of 100-bp trees in 10-kb windows in which *M. vitellinus* is sister to *aurantiacus*, which is the expected topology in a gene flow scenario. Trees included *M. vitellinus*, *M. aurantiacus*, *M. candei*, and trans-Andean *M. manacus*. (**I**) f_d and (**J**) gene flow topologies from (H) calculated in 2-kb windows in the region surrounding *BCO2*. The pink shaded regions correspond to the *vitellinus*-to-*candei* introgression block denoted by bold black lines in Fig. 3I.

The impact of feather microstructure on carotenoid coloration is understudied, but the common co-occurrence of feather carotenoids with wide barbs lacking barbules has been known for decades (*62*). In accordance with these previous observations, we found wider barbs and reduced barbules in *Manacus* collar feathers containing lutein and a significant positive relationship between barb width and lutein concentration. It is unclear whether these feathers develop without barbules, or if the barbules are gradually lost throughout the season, as both processes have been observed (*63*, *64*). Lutein deposition in yellow feathers may inhibit full formation of hierarchical feather structure (*63*), but our results suggest that it is not the sole factor causing structural differences in *Manacus* feathers. Collar feathers of *vitellinus* had lutein concentrations similar to hybrid collars and *candei* bellies, but both of the latter retained

more barbules than *vitellinus* collars. We also found that feather microstructure, including barb width and, potentially, barbule morphology, affect color by shifting peak reflectance toward redder hues and increasing color saturation and purity. These results suggest that altering feather microstructure may be an important component of birds' color signaling and that this process is likely refined by selection. Barb shape, including greater width and flatness, has previously been shown to increase color saturation in other birds (*65*), and a lack of barbules has been hypothesized to reduce diffuse scattering of light (*63*). Further analysis of morphological data in manakins and other species, including more quantitative barbule measurement, will improve tests of this hypothesis. Populations that have received introgression resulting in de novo deposition of carotenoids, as in the manakin hybrid zone, are particularly fruitful systems in which to conduct such tests.

Genetic basis of plumage color

Three complementary genomic approaches, dSNPs, RADseq clines, and sliding window differentiation and introgression metrics, all identified alleles around and within the gene *BCO2* as the major genetic difference between cross-river manakin populations that differ in collar color (Fig. 3). These analyses also confirmed that, in yellow-collared hybrid populations, the block of DNA containing *BCO2* is derived from *M. vitellinus* and reached admixed populations via introgression. A growing body of evidence has pointed to *BCO2* as a common target of selection controlling simple carotenoid-based color differences in the integument of many vertebrates, including salmon flesh (*51*), mammal fat (*45*), lizard skin (*50*), bird bare parts (*48*, *52*, *66*), and bird feathers (*46*, *47*). *BCO2* alleles also appear to have spread between colorful species several times in parulid warblers (*49*).

When BCO2 is active, it cleaves carotenoids into colorless products (*37*). As a result, changes to *BCO2* that result in greater carotenoid content typically involve loss-of-function mutations (*45*, *66*) or reduced expression (*47*, *48*, *50*). We found no differences between the *BCO2* coding sequences of yellow- and white-collared males, so loss of function at the protein level is unlikely. Nevertheless, the signal of introgression was localized in and around the gene, thus pointing to a mutation or mutations in cis-regulatory elements in an intron or flanking sequence as the most likely genetic cause of the yellow phenotype. Although *BCO2* expression was lower in *M. vitellinus* muscle than several relatives, its expression in the cerebellum appeared to be higher (fig. S34). Therefore, we favor a hypothesis involving precisely localized and/or timed reduction in gene expression or enzyme activity during feather development. Such tissue-specific gene expression regulates other sexual traits in manakins (*67*), and skin-specific control of *BCO2* expression underlies the yellow skin of domestic chickens (*48*). Gene expression analysis in growing feathers, liver, kidney, gut, and other tissues involved in carotenoid processing and deposition is needed to address this hypothesis.

Several other genes were identified by one or a combination of analyses that point to other instances of introgression across the *Manacus* hybrid zone, including *ASIP*, *RDH10*, and *RSPO2*. Whether any of these genes are causally related to introgressing plumage or behavioral traits deserves further study.

Historical gene flow at *BCO2*

We also identified historical introgression at *BCO2* between *M. aurantiacus* and *M. vitellinus*. Allele frequency patterns showed a strong introgression signal at *BCO2* between the two species, and the topology of the well-supported *BCO2* gene tree suggests that the allele for pigmented collars arose in *aurantiacus* and spread to *vitellinus*. While incomplete lineage sorting can also produce gene trees that do not match the species tree, we consider it unlikely to be the cause of the *BCO2* gene tree topology. Incomplete lineage sorting is most likely when internodes are short (*68*), but this is not the case for *Manacus* (*69*). In the study of Leite *et al.* (*69*), all marker types (ultraconserved elements and exons) and analytical methods (concatenation and gene tree reconciliation) strongly supported the sister relationship between *candei* and *aurantiacus*. *M. vitellinus* and *aurantiacus* are not now in contact, but they are separated by ~25 km in central Panama (*58*, *59*) and could have hybridized in the past. While we cannot identify the phenotypic outcome of this introgression with the same confidence as the *vitellinus-candei* introgression, a combination of evidence strongly supports the notion that *BCO2* introgression from *aurantiacus* to *vitellinus* had an important impact on *vitellinus* coloration. This evidence includes the connection we discovered between *BCO2* and *vitellinus* coloration, the known importance of *BCO2* to plumage color in other species (*46*, *47*), the known importance of collar color for sexual selection in *Manacus* (*27*, *28*), and the fact that the signal of introgression from *aurantiacus* to *vitellinus* largely overlaps with the *vitellinus*-to-*candei* introgression block. The most likely scenario, therefore, is one in which the *BCO2* allele for pigmented collars arose once in *M. aurantiacus*, was subsequently transferred through hybridization to *vitellinus*, spread throughout its range, and then partially spread into a third species, *M. candei*, in western Panama.

Three-species introgression has rarely been reported in nature (*70*–*77*). Even rarer are instances in which such introgression is clearly connected to positive selection for the movement of traits between species, as occurred with the spread of seasonal camouflage pelage among rabbits (*76*) and, most likely, colorful plumage in *Setophaga* warblers (*49*). Multispecies introgression may be common early in rapid radiations like those of African cichlids (*77*), *Heliconius* butterflies (*78*), and Andean siskins (*79*). Whether situations like the present one involving sexually selected traits are common awaits further study, and the continued advance of genomic technologies and methods will facilitate that process.

Sexual selection: What traits and which mechanisms?

The asymmetric introgression of adult male plumage traits in *Manacus* has been attributed to female choice and/or male-male competition [reviewed in (*32*)]. In a study on mixed leks with both yellow- and white-collared males, Stein and Uy (*28*) found that yellow-collared males received more visits from females and copulated more often than white-collared males, implicating female choice in the plumage introgression. Supporting the male-male competition hypothesis, McDonald *et al.* (*30*) showed that yellow-collared manakin males, whether pure *M. vitellinus* or hybrids, were more physically aggressive than white-collared birds, which likely confers an advantage during dominance interactions. However, since yellow collars and olive-green bellies were correlated in their study populations, it is plausible that belly color was the plumage trait directly associated with increased aggression in that study. Stein and Uy (*28*), in a similar study on mixed-color leks, did not detect a difference in aggression between yellow- and white-collared males, but this study also did not control for belly color. We have shown here that the darker olive-green belly colors of *vitellinus* and some hybrids result from the deposition of melanosomes in feather barbules. In a number of

vertebrate systems, melanocortins have been known to produce pleiotropic effects on both coloration and behavior, with darker coloration often associated with greater aggression, especially in birds (*80*). Of note, Long *et al.* (*29*) recently showed that olive green belly color, while initially trailing yellow collars in the *Manacus* system, has continued to spread into admixed populations and has reached the Río Changuinola within the past 30 years. Thus, yellow collars, olive bellies, and enhanced aggressiveness may all be targets of sexual selection in this system, and their relative importance remains to be determined.

In combination with previous results, evidence presented here that colorful collars likely originated in *M. aurantiacus* and spread to *vitellinus* before reaching the *vitellinus* x *candei* hybrid zone and spreading into *candei* populations supports the hypothesis that colorful collars are generally attractive within *Manacus*. Positive selection on carotenoid-based plumage colors is implicated in other bird systems, such as the multiple cross-species introgressions of *BCO2* among *Setophaga* warblers (*49*), the asymmetrical introgression of red plumage in fairy-wrens (*14*), and the attractiveness of brighter red plumage in house finches (*20*). Selection for more intense colors has been interpreted as potentially resulting from honest signaling for higher male quality (*81*) or perceptual bias for particular signals (*19*). These explanations for yellow plumage introgression would predict that it should continue to spread whenever possible.

In *Manacus*, therefore, the fact that plumage introgression from *M. vitellinus* into *candei* appears to have been stalled for more than 30 years at the Río Changuinola (*29*) and has not swept through trans-Andean *M. manacus* populations despite two apparent contact zones in Colombia (Fig. 1A) (*82*) presents a conundrum. Several explanations for stalled introgression have been proposed, including the river acting as a barrier to gene flow, positive frequency-dependent selection for yellow, variable light environments, or a combination of these factors (*23*, *28*, *83*). To date, none of these proposals is supported by convincing evidence (*32*). A recent model of mate choice focused on how females acquire mating preferences predicts that, under certain conditions, female preference will vary over time and space (*84*). This possibility also deserves consideration in the *Manacus* system. Evidence from the present study linking *BCO2* to collar color variation in the hybrid zone should facilitate further detailed investigation of the evolutionary mechanisms acting on color in *Manacus*.

Do colorful collars come at a cost?

We hypothesize that the spread of carotenoid-pigmented collars, while clearly advantageous for sexual selection in some cases, may come at a fitness cost for natural selection. We have shown here that microstructural modifications accompany lutein pigmentation in *Manacus* collar feathers and are likely to affect their physical performance in shedding water (see Materials and Methods for further discussion of the water repellency model). Water shedding is a critical function of feathers in the tropical rainforests where manakins live. The potential negative fitness effects of reduced water shedding capacity are numerous and varied (*85*). Our estimates of water repellency predict that *Manacus* species with pigmented collar feathers have significantly reduced water shedding performance compared to species with white collars. Lower predicted water repellency is due to the wider barbs of pigmented feathers, which reduce pore size and increase the ratio of solid surface to air in contact with water droplets, reducing net surface tension and enhancing wettability of feathers (*34*). Water repellency of hybrid collars spanned nearly the entire range of values for white and pigmented collars (Fig. 2G), suggesting that individuals at the lower end of this range may incur a fitness cost (*86*) in the hybrid zone in western Panama, an area where rainfall is extremely high (*87*).

Collar width is another trait that has introgressed asymmetrically along with carotenoid pigmentation in this hybrid zone (*13*). The pigmented collar on the dorsal surface (hindneck) of *M. vitellinus* is much narrower than the white dorsal collar of *M. candei* (Fig. 5). We speculate that this narrow hindneck collar trait may compensate for the reduced water repellency of lutein-pigmented collar feathers, limiting potential negative impacts of their reduced water shedding capacity. Previous work demonstrated that the narrow dorsal collar of *vitellinus* has partially introgressed into hybrid populations but trails behind the limit of yellow collar introgression (*13*). Hybrids at site 4 on the east bank of the Río Changuinola have bright yellow collars like *M. vitellinus*, but their dorsal collar width is very broad like *M. candei* (Fig. 5). It is possible that hybrids with this combination of traits may experience negative fitness effects due to reduced water shedding capacity of their broad yellow collars. Natural selection may act to ameliorate this cost by reducing the width of the dorsal collar, driving the observed introgression of narrow collars from *vitellinus* into *candei*. Future studies could test this idea by examining the physiological effects of intense rainfall on hybrid manakins with different combinations of these traits.

We note that our water repellency estimates are based on a simple model originally designed to estimate the water shedding capacity of porous textiles (*34*, *35*). A recent review details complexities of feather structure that are not captured by this model and emphasizes the likely importance of barbule microstructure in water repellency (*88*). While barbule microstructure is not considered in our model estimates, it seems likely that the absence of barbules on the distal third of pigmented *Manacus* collar feathers would only increase their wettability, reinforcing the conclusions reached here.

In sum, our results show that a case of asymmetric sexual trait introgression in the manakin genus *Manacus* likely results from a regulatory change in the carotenoid processing gene *BCO2* and that this introgression was preceded by historical gene flow at the same gene from a third species in the genus. Such three-species introgression events may be more common than now appreciated early in radiations, but reported cases involving key traits, like coloration in a lekking bird, have so far been rare. We show that the

Fig. 5. Collar width differences between *M. vitellinus*, *M. candei*, and their hybrids. Specimens with representative dorsal collars from the hybrid zone region were photographed: *M. vitellinus* are from site 10, hybrids are from site 4, and *M. candei* are from site 2. Yellow feathers have reduced water shedding capacity relative to white feathers, so we propose that the narrow collar of *M. vitellinus* may compensate by reducing the available wettable surface.

microstructure of carotenoid-pigmented feathers has likely been refined by selection to enhance coloration, and we propose both a potential fitness detriment that results from those modifications and a potential compensatory mechanism. These findings reveal the intricate interplay of sexual selection, hybridization, and introgression involved in shaping the ornamentation and behavior of these birds and hint at additional levels of complexity yet to be explored.

MATERIALS AND METHODS

Feather color and pigment analysis

We examined the collar and belly feathers of four species in the genus *Manacus* (*M. manacus*, *M. candei*, *M. vitellinus*, and *M. aurantiacus*), as well as from *M. candei* x *M. vitellinus* hybrids. Five feathers were plucked from each of two plumage patches, the belly and collar, of six museum specimens of each taxon from the US National Museum of Natural History (NMNH). Specimen information is available in table S1. We used a combination of light microscopy, reflectance spectroscopy, and HPLC to characterize the pigments in feathers and the mechanisms of color production. We sought to determine which carotenoids were present and their concentrations and to visually determine the presence and location of melanin in feather morphology.

Each feather was examined under reflected light before and after carotenoid extraction. The presence or absence of barbules along the barbs and the presence of pigmentation (carotenoids and/or melanization) in the barbs and barbules were noted. Pictures were taken using an AmScope Microscope Digital Camera at a magnification of ×10 and ×40.

When performing UV-visible spectroscopy, five feathers were overlapped and taped down flat, ventral side up, onto a black cardboard background. This was done to simulate how the feathers may have been placed on the bird during life and to eliminate any background noise when sampling the feathers. Three measurements were taken in a dark room at a 90° angle of incidence from each set of feathers using an Ocean Optics USB4000 spectrophotometer and an Ocean Optics PX-2 pulsed xenon light source relative to a white reflectance standard (Labsphere Inc., North Sutton, NH, USA). Spectra were measured using OceanView v1.67 (Ocean Insight, FL, USA). Spectral measurements were taken from the left, center, and right of the distal end of the overlapped group of feathers. Capturing multiple measurements from each plumage patch helps account for any variation in color within or between feathers. The resulting spectral data were analyzed and graphed using the pavo package v. 2.4.0 (*33*) in R v. 4.3.3 (*89*).

For carotenoid analysis, we sampled two feathers in each feather patch from each species and hybrids. All feathers were cut approximately one-third of the way up from the base, removing the bottom portion of the feather that was heavily melanized and saving the top two-thirds of the feather. Carotenoids were extracted from cut feather sections and analyzed using HPLC. See Supplementary Text for detailed methods.

We performed statistical analyses of feather data in R using linear models corrected for multiple comparisons using the emmeans package v.1.4.5 (*90*) and linear mixed effects models. First, we compared the concentration of lutein (square root transformed to achieve normality) in the belly or collar feathers among the five species and hybrid included in this study. Next, we compared the concentration of lutein in the belly versus the collar feathers of the three taxa which had yellow pigmentation in both feather patches (hybrids, *M. vitellinus*, and *M. aurantiacus*). Next, we investigated the effect of increasing lutein concentration on colorimetric variables obtained during reflectance spectroscopy of collar feathers only (to remove the effect of barbule morphology present in belly feathers) using a mixed effects model that incorporated specimen identity to account for non-independence of data within species/hybrid form. These variables were saturation in the yellow wavelengths of light (S1yellow), UV reflectance saturation (S1UV), carotenoid chroma (S9), mean sample brightness (B2), and sample midwavelength hue (H3). Next, we compared feather brightness (as measured by reflectance spectroscopy) of collar feathers of each of the five taxa. Next, we modeled the relationship between barb width and lutein concentration and between barb width and the colorimetric variables described above. Last, we compared the concentration of lutein and the colorimetric variables above between yellow belly feathers of *M. candei* and yellow collar feathers of *M. vitellinus* and hybrids.

From each model analysis, we report the estimated effect size (β: the difference between groups or the slope of the relationship between two variables), the confidence interval around the estimated effect size, and the associated *P* value (Table 1 and tables S2 and S3). All supplemental feather figures and graphs were built in R using the ggpubr v.0.2.1 (*91*) and cowplot v.1.0.0 (*92*) packages.

Generation of genome resequencing data and reference-based scaffolding

Samples used for genome resequencing were collected in northwest or central Panama. All birds were collected in 1980–1990s and preserved as voucher specimens at the US Museum of Natural History as round or flat study skins or skeletal specimens. All samples were previously studied by Brumfield *et al.* (*23*), so we follow their population/site designations for consistency. We sequenced 12 *M. candei*, 4 *M. vitellinus*, and 10 hybrids from a population with a predominantly *candei* genomic background but some introgression from *vitellinus* (table S5). Two *M. candei* individuals represented parentals from site 2 near the border with Costa Rica and 10 were from site 3 on the west bank of the Río Changuinola (Fig. 1C). The 10 hybrids were from site 4 on the east bank of the Río Changuinola (Fig. 1C). The four parental *M. vitellinus* were from site 12, ~250 km east of the Rio Changuinola, far from the plumage or genomic contact zones (Fig. 1C). Collar and belly plumage color of the birds from sites 3 and 4 was confirmed by examining the museum specimens. DNA, extracted through a phenol-chloroform and ethanol precipitation method, was shipped to the McDonnell Genome Institute, Washington University for library preparation and DNA sequencing across three lanes of the Illumina HiSeq X platform (2 × 150 bp paired-end reads). Raw sequencing reads are available from National Center for Biotechnology Information (NCBI) at BioProject PRJNA1129471.

The average number of raw FASTQ reads per individual was 97.6 million (range: 64.4 to 123.6 million). We used Cutadapt implemented in Trim Galore v0.6.4 (https://github.com/FelixKrueger/TrimGalore) to conduct quality and adapter trimming (default parameters). The average read length and number of reads per sample after quality trimming were 145.4 bp and 96.3 million (range: 63.7 to 121.6 million), respectively. We used bowtie2 v2.3.5 (*93*) to map trimmed and filtered reads to the annotated reference genome of *M. vitellinus* (NCBI RefSeq accession GCF_001715985.3). At the time of read mapping, this reference genome was the only one

available for the genus. Samtools v1.9 was then used to sort and index the bam files (*94*). This reference genome (scaffold N50 = 17.9 Mbp, contig N50 = 290.6 kbp) was generated with a combination of Illumina HiSeq short reads and Pacific Biosystem long reads and assembled with MaSuRCA v3.1.1 (*95*).

Across all samples, the average overall botwtie2 alignment rate was 94.6% (range: 91.5 to 96.5%). Next, we followed recommended best practices and used GATK v3.8.1 to conduct variant calling (*96*). Briefly, we used the HaplotypeCaller tool to conduct calling of SNPs and insertions/deletions (indels) simultaneously via local de novo assembly of haplotypes. This generated per-sample intermediate GVCF files, which were then combined with the GenotypeGVCFs tool to produce the final raw VCF file. We then selected for SNPs and used the GATK tool VariantFiltration to conduct both SNP- and genotype-level filtering. We used the expressions "QualByDepth < 2.0 || FisherStrand > 60.0 || StrandOddsRatio > 3.0 || RMSMappingQuality < 40.0 || ReadPosRankSum < −3.0 || ReadPosRankSum > 3.0 || BaseQRankSum < −3.0 || BaseQRankSum > 3.0 || MQRankSum < −3.0 || MQRankSum > 3.0" and "DP < 5.0 || GQ < 13.0" to remove low-quality or spurious SNPs and genotypes, respectively, during the filtering process. Last, we retained SNPs that contained genotype information in at least 21 individuals (of the total 26), producing a filtered VCF file containing 19.8 million SNPs. At the individual level, the proportion of SNPs with missing genotype information ranged from 2.9 to 22.5% (table S3).

Because a downstream analysis (ABBA-BABA analysis) required the use of an outgroup taxon to determine derived-ancestral allelic states, we downloaded Illumina HiSeq 2000 FASTQ reads from a whole-genome sequencing project of *Pipra filicauda* (NCBI Run Accession: SRR6885520; 105.5×10^{12} bp, 349.2×10^{6} 150 bp paired-end reads). Following the above workflow, we mapped *P. filicauda* reads to the *M. vitellinus* reference genome and generated a separate VCF file with outgroup data. This VCF contained 44.5 million SNPs after SNP-level, genotype-level, and missingness filtering.

To place *M. vitellinus* scaffolds in their approximate chromosomal positions, we conducted reference-guided chromosome-level scaffolding, using the genome of *C. lanceolata* (lance-tailed manakin) as the reference (NCBI RefSeq accession GCF_009829145.1). This high-quality genome assembly consisted of full chromosomes, including 33 autosomal macro- and microchromosomes, and two sex chromosomes (W and Z). We used RaGOO v1 (*97*) with default parameters to conduct scaffolding. As expected, given the high level of synteny among bird species, the scaffolding process resulted in high confidence in terms of placing and orienting each *M. vitellinus* scaffold against *C. lanceolata* chromosomes (average positional confidence score = 77.8%, SD = 27.6%; average orientation confidence score = 98.2%, SD = 7.3%).

Principal components and phylogenetic network analysis

To reveal relative divergence among populations and evolutionary relationships among individuals, we conducted phylogenetic network analysis using the NeighborNet algorithm implemented in SplitsTree v5 (*98*, *99*). We took the above filtered VCF file containing 19.8 million SNPs and removed SNPs with minor allele frequency of less than 5%. This was followed by thinning of SNPs so that no two sites were within 10,000 bp of each other. This produced a final VCF file containing 103,885 SNPs. Using PGDSpider v2.1.1.5 (*100*), we converted the reduced VCF file into a FASTA file (one sequence per individual) while collapsing heterozygous genotypes into International Union of Pure and Applied Chemistry ambiguity codes. Before NeighborNet network construction, we used the HKY85 substitution model, a model appropriate for closely related species, to calculate genetic distances among individuals. To simplify the network, we filtered edges by setting maximum dimension to 4 (i.e., removing splits that caused boxes in the network to have dimensions > 4).

To conduct principal components analysis, we first used ANGSD v0.918 to generate filtered genotype posterior probabilities (command: -doMaf 1 -doMajorMinor 1 -SNP_pval 1e-6 -uniqueOnly 1 -remove_bads 1 -only_propoer_pairs 1 -C 50 – baq 1 -minMapQ 20 -minQ 13 -minMaf 0.05 -minind 21 -GL 1 -doGeno 32 -doPost 1) (*101*). Only SNPs with data in at least 21 of 26 individuals and a minimum allele frequency of 5% were kept. This created a genotype posterior probabilities output containing 13.1 million SNPs. Following this, we used ngsCovar v1 to randomly subsample 1 million SNPs to reduce linkage disequilibrium and to calculate the covariance matrix among individuals (*102*). Eigenvector decomposition was then conducted in the R statistical package to generate the principal components (*89*).

Modeling population divergence and gene flow

Using the genome resequencing data and an allele frequency spectrum approach, we estimated population divergence histories between *M. vitellinus* ($N = 4$), *M. candei* ($N = 10$, site 3 only), and hybrids ($N = 10$, site 4) and between the latter two populations only (table S3). For the three-population analysis, we removed any SNPs that have missing data across the three populations, creating a full data matrix. Following this, we kept only SNPs that were at least 1000 bp from each other to reduce linkage disequilibrium among them. This resulted in a folded three-dimensional (3D) site frequency spectrum that contained 608,905 segregating sites. Next, we modified an optimization routine (moments_Run_Optimizations.py) in moments_pipeline (github.com/dportik/moments_pipeline) to evaluate the fit of five candidate population divergence models (table S6 and fig. S6) to the data. The population branching history of all three-population models was (*M. vitellinus,* (*M. candei,* hybrids)), and the tested models varied with respective to whether migration was allowed between pairs of populations. The lower and upper bounds of population size (0, 40), time of split (0.0001, 10), and migration rate (0, 50) parameters were kept the same when testing all models. These parameter bounds have been verified to be appropriate through multiple preliminary moments runs.

After the preliminary runs were completed, for each demographic model being tested, we first conducted four to five independent moments_pipeline optimization runs, with each run containing four sequential rounds and each round containing 10 (round 1) or 20 (rounds 2 to 4) independent replicate moments runs. While starting parameters of the first-round replicates were random, parameters from the best scoring replicate after each round was completed were used to initiate perturbed starting parameters for replicates of the subsequent round. The levels of perturbation of starting values (i.e., "fold" value) for the four sequential rounds were 3, 2, 1, and 1, respectively.

When parameter optimization of each model was completed, we inspected log likelihood values across runs to ensure convergence. After all candidate models were evaluated with moments_pipeline, we then used the Akaike information criterion to select the best demographic model. Using this best demographic model, we conducted one final, long moments run (maximum number of iterations =

100), using demographic parameters from the best round 4 moments_ pipeline replicate as starting values. To estimate parameter uncertainties, we first generated 100 bootstrapped folded spectra and used the Godambe Information matrix, an appropriate approach for composite likelihoods and SNPs that are not fully unlinked, to calculate 95% confidence intervals (*103*).

The same optimization and modeling approaches were applied to a 2D site frequency spectrum between *M. candei* from site 3 and hybrids from site 4 (number of segregating sites = 399,572). We tested four candidate models that varied with respect to whether or when migration occurred between the two populations (table S6). To convert substitution rate–scaled parameter estimates to absolute units, we used a genome-wide substitution rate of 3.3×10^{-9} substitutions/year and a generation time of 2.5 years.

Genomic window-based divergence and introgression metrics

Because of our sampling scheme along the Río Changuinola—very similar populations genetically but with a major color difference—we expected genomic regions underlying color to show strong signals of both differentiation across the river and introgression from *M. vitellinus*. To locate these regions, we calculated differentiation and introgression statistics in sliding windows along genomic scaffolds. Because any single population genetic statistic may be affected by confounding factors and because we expected a region underlying color to be robust to such issues, we used multiple analysis methods to assess both differentiation and introgression (*40*, *41*). We calculated these statistics in non-overlapping windows of 10, 25, and 50 kb (fig. S35). Results were similar between window sizes, and the smallest size allowed us to narrow down regions of interest more precisely. For that reason, we used 10-kb windows in downstream analyses and present those results in Fig. 3. We omitted all scaffolds smaller than 10 kb, which accounted for 0.25% of the total genome length. We identified focal regions potentially underlying the plumage color difference by selecting windows that fall above the 99.9th percentile of the differentiation and introgression statistics (described below). The avian Z chromosome has a smaller effective population size than autosomes (macro- and microchromosomes), and as a result, differentiation and introgression statistics behaved differently on Z than on autosomes (fig. S36). Therefore, we calculated Z chromosome 99.9th percentile thresholds separately from autosome thresholds.

We predicted that genomic regions underlying the plumage color differences between *M. vitellinus* and *M. candei* would show substantial genetic differentiation between birds from sites 3 and 4 on either side of the Río Changuinola (Fig. 1C and table S3). We used the popgenWindows.py script (github.com/simonhmartin/genomics_general) to calculate the nucleotide diversity, π, of each population, the fixation index, F_{ST}, and sequence divergence, D_{XY} (*42*), between the two populations. F_{ST} is the proportion of total genetic variation accounted for by differences between populations, while D_{XY} is the average of the pairwise sequence divergence between population samples. The method we used calculates variant site measures of D_{XY} and π, so we calculated invariant sites in each window and adjusted D_{XY} and π values accordingly (see get.popgen.data.R in Supplementary Code for details). Because D_{XY} is heavily influenced by nucleotide diversity, π, (Pearson's $r = 0.984$; fig. S37A), we instead used D_a (*42*) for downstream analyses, which we calculated by subtracting the mean π of the two populations from D_{XY} (fig. S37B).

Because the plumage differences between *M. candei* and hybrids are likely due to introgression of these traits from *M. vitellinus* into the hybrid population (*13*, *23*), we calculated introgression statistics to identify genomic regions in hybrids that originated in *M. vitellinus*. We predicted that regions underlying the plumage color differences would show signatures of both differentiation and introgression. We calculated f_d, which is a modified version of the ABBA-BABA *D* statistic intended to be applied to population samples in small genomic windows using the ABBABABAwindows.py script (github.com/simonhmartin/genomics_general) (*43*). f_d is an estimator of the proportion of a genomic region that is shared due to introgression between populations P2 and P3 in a set of populations with the relationship (((P1, P2), P3), O). f_d is a more sensitive and less biased statistic than *D* when applied to small genomic regions (*43*), and unlike F_{ST} and D_a, f_d is not sensitive to local recombination rate variation since it depends on the ratio of various allelic states across a tree rather than measures of genetic diversity (*104*). In our calculations, we used P1 = *M. candei* (site 3, $N = 10$), P2 = hybrids (site 4, $N = 10$), and P3 = *M. vitellinus* (site 12, $N = 4$), and the outgroup was *P. filicauda*. We omitted windows with fewer than 100 biallelic SNPs used to calculate f_d, as recommended by the author of ABBA-BABAwindows.py.

In addition to f_d, we estimated the RND of the split between site 3 *M. candei* and site 4 hybrids to the split between hybrids and *M. vitellinus* (site 12) by calculating sites 3 to 4 D_{XY} ÷ sites 4 to 12 D_{XY} (*44*). Assuming a consistent substitution rate across lineages, values greater than one represent genomic windows where the divergence between hybrids and *M. vitellinus* is more recent than the hybrid/*M. candei* divergence. Because the genomes of hybrids are predominantly derived from *M. candei* (*23*, *29*, *36*), these windows should be very rare in the genome and indicate introgression from *vitellinus*.

A total of 266 autosomal (of 91,913) and 26 Z chromosome (of 7079) 10-kb windows were considered 99.9th percentile outliers for at least one of the four summary statistics. A substantial proportion of these windows were flagged as outliers by two or more summary statistics (autosomes: 32.3%; Z chromosome: 23.1%) (fig. S9). Among the windows flagged by two summary statistics ($n = 75$), the majority were flagged by either the two introgression statistics, f_d and RND (autosomes: 37 of 75; Z chromosome: 4 of 6), or the two differentiation statistics, F_{ST} and D_a (autosomes: 36 of 75; Z chromosome: 1 of 6). The fact that outlier windows for introgression statistics did not often overlap with differentiation statistics outliers suggests that high differentiation (between hybrids and *M. candei* in site 3) of some windows might have arisen from processes other than introgression (from *M. vitellinus* into hybrids), including local selection or drift in one of the two *M. candei* populations after their lineages diverged or increased F_{ST} or D_a due to low π and/or recombination rates (*104*). Nevertheless, a number of autosomal outlier windows were supported by three or all four summary statistics, indicating that these were strong candidates for windows containing loci that underlie the plumage introgression (fig. S9).

To facilitate the inspection of gene content of genomic regions that received strong support from our window-based analyses, we selected focal windows based on the following approach. We considered an autosomal window (window size = 10 kb) a focal window if it was marked as a 99.9th percentile outlier by at least three of the four summary statistics (num_outliers ≥ 3). In addition, we used the rollmean function of the R package zoo (*105*) to calculate centered

moving average of num_outliers; for each window, we calculated the average of its num_outliers and those of the two windows that were immediately up or downstream (MAV3). Next, an autosomal window was considered a focal window if its num_outliers ≥ 3 or MAV3 ≥ 1. The use of moving averages as a criterion for identifying focal windows allowed us to find genomic regions of interest where outlier windows for the various introgression/differentiation statistics were not exactly coincident but could be found in adjacent windows. Because no Z chromosome windows had num_outliers ≥ 3 (fig. S9B), the following criteria were used to identify focal windows: num_outliers ≥ 2 or MAV3 ≥ 1.

Using these criteria, we found a total of 74 and 8 focal windows in autosomes and the Z chromosome, respectively. We further organized the focal windows into 24 genomic neighborhoods where focal windows were contiguous or no more than 1000 kb (100-window length) from each other (table S10 and figs. S10 to S33). These genomic neighborhoods were found only in six autosomes and the Z chromosome. They each spanned 10 to 960 kb, containing zero to eight *ab initio* annotated protein coding genes. Three such genomic neighborhoods stood out as being highly prominent in that they each contained one (genomic neighborhood 11) or two (genomic neighborhoods 9 and 19) 10-kb windows that were outliers for all four summary statistics (table S10). A list of genes, and their functions, found in strongly supported windows can be found in table S11.

Pathway and gene ontology term overrepresentation analysis

To test whether the outlier-marked regions of the genome were enriched with genes from defined molecular pathways or functions, we used the Protein Analysis Through Evolutionary Relationships (PANTHER) classification system (*106*). We filtered the *M. vitellinus* reference genome for isomers annotated under multiple protein IDs and consolidated to a single isomer per gene. The filtered *M. vitellinus* reference genome amino acid sequences for all proteins were queried against the PANTHER hidden Markov model library using the hmmscan option to return the best hit (*107*). Once functional classifications were obtained for as many of the proteins in the genome as possible, genes (again, filtered down to single isomer representation) that appeared within a 10-kb outlier window supported by any of the four differentiation or introgression statistics or 20 kb up- or downstream of the outlier window were defined as the outlier subset from the full genome complement of proteins. We chose an additional area that was ±20 kb of the outlier window because it could contain a distal cis-regulatory element (e.g., enhancer and insulator) with its associated gene.

We used the PANTHER Gene List Analysis tool to perform a PANTHER pathways statistical overrepresentation test; in short, the functional classifications for the entire genome complement served as a basis for expected composition of an outlier subset. Without pathway enrichment, one would expect to observe the same proportion of genes from a given pathway in a subset as are present in the entire genome complement. Statistical deviation from expected values in our observed outlier gene set was assessed with a Fisher's exact test including a false discover rate correction for multiple tests. We also used the PANTHER gene list analysis tool to assess whether any GO-Slim (Gene Ontology Slim) term categories (molecular function) were overrepresented in the same manner as the pathways.

Cline analysis

We sought to increase the geographic resolution of our introgression results by fitting geographic clines to phenotypic traits SNPs genotyped using RADseq from additional sampling sites in the *Manacus* distribution. We sequenced 152 individuals from eight sites (Fig. 1C, sites 2 to 10) to capture variation in hybrid as well as parental populations, following the sampling transect from (*23*). The locations and sample sizes of each site are available in table S14. For phenotypic clines, we measured three male traits (beard length, collar color, and belly color) using the whole museum skins of male *Manacus* manakins that were measured by (*23*) and deposited at NMNH. Detailed methods are described in (*29*). For the genetic clines, we used DNA samples archived at NMNH from individuals captured by Parsons *et al.* (*13*) and Brumfield *et al.* (*23*) and then sequenced in (*29*). Detailed methods on DNA extraction, sequencing, SNP calling, filtering, including cline width credibility interval filters, and genetic and phenotypic cline fitting are described in (*29*) following the methods for the "historical" dataset. Our final SNP cline dataset consisted of 4750 geographic clines with precise cline centers. Raw reads are available at NCBI BioProject PRJNA893627.

BCO2 expression

We explored *Manacus* lineage–specific gene expression of *BCO2* using gene expression data from scapulohumeralis and pectoralis muscles in six species of manakins and a suboscine outgroup from (*67*). Muscle reads were mapped to the *P. filicauda* genome (GCF_003945595.1) using the splice aware-aligner STAR v 2.7 (*108*) and counted against gene features using featureCounts v2.0.1 (*109*). Data on *BCO2* expression in cerebellum came from three manakin species and a suboscine outgroup (table S16). Cerebellums were collected from breeding males of each species, and RNA was extracted using a Qiagen RNeasy kit and sequenced in 2 × 100 bp reads on an Illumina NextSeq 500. Reads are available at NCBI BioProject PRJNA321179. Cerebellum reads counts were estimated using kallisto, using 30 sample bootstraps and transcripts available for *M. vitellinus* (GCF_001715985.3), and converted to counts using R package tximport. We compared lineage-specific gene expression in these muscle and brain tissues using PhyDGET. This method assigns Bayes factors (>|1.5|) to infer significant changes in gene expression along specific branches.

Historical *BCO2* gene flow in *Manacus*

We prepared whole-genome sequencing libraries for nine additional individuals to encompass the major lineages within *Manacus*, including three *M. aurantiacus*, three *M. manacus* from east of the Andes (cis-Andean), and three *M. manacus* from west of the Andes (trans-Andean) (table S15). The libraries were sequenced by Novogene Corp. on one Illumina HiSeq lane, producing 217 million total reads averaging 23.8 million reads per sample. Raw sequencing reads are available from NCBI at BioProject PRJNA1129471. Reads were trimmed using Cutadapt implemented in Trim Galore and aligned to the *M. vitellinus* reference genome using bwa mem (*110*). We marked duplicates using picard MarkDuplicates. We followed the GATK best practices workflow for variant calling, including producing and filtering a VCF file, and then used the filtered VCF to apply a recalibration table to the original bam files using GATK v3.8.1.0 (*96*). The terms we used for removing low-quality or spurious SNPs and genotypes were "QD < 2.0 || FS > 60.0 || SOR > 3.0 || MQ < 40.0 || ReadPosRankSum < −3.0 ||

ReadPosRankSum > 3.0 || BaseQRankSum < −3.0 || BaseQRankSum > 3.0 || MQRankSum < −3.0 || MQRankSum > 3.0" and "DP < 4.0 || DP > 45.0 || GQ < 3.0," followed by a filter to remove indels and sites missing in more than five of nine individuals in VCFtools v0.1.16 (*111*).

We selected two control genes on chromosome 24 similar in size to *BCO2*, more than 1 Mb away, and with no known connection to coloration, *DCPS* and *TBCEL*. Our rationale was to determine whether any introgression signal we detected at *BCO2* was independent of its genomic context. We identified genomic regions to use for building gene trees by anchoring the ends of the regions of interest in exons of flanking genes to aid sequence alignment. We used a much shorter sequence for the *BCO2* gene tree (48 kb, from 26 kb upstream to 5 kb downstream) than the control trees (306 and 384 kb, respectively) because of the likelihood that recombination has reduced signals of shared ancestry that may have been present if introgression occurred at *BCO2*.

Using bam files from each individual, including two *M. candei* and four *M. vitellinus* whole-genome resequencing samples used in the above analyses, we produced a single consensus sequence per individual using Samtools consensus (*94*) and then aligned the sequences using Mafft (*112*). To facilitate tree rooting, we included the corresponding genomic regions from the reference genomes of *P. filicauda* (accession ASM394559v2) and *C. lanceolata* (Accession bChiLan1.pri) in the alignments.

We used IQ-Tree v2 (*113*) to produce maximum likelihood gene trees from each alignment with 10,000 bootstrap replicates, and in each case, we allowed IQ-Tree to select the best model of sequence evolution using Bayesian information criterion. The resulting trees were rooted at the midpoints.

Next, to place the evidence of gene flow at *BCO2* in the context of genome-wide signals of introgression between *M. aurantiacus* and *M. vitellinus*, we calculated ABBA-BABA *D* statistics. To produce a VCF file for this analysis containing all species, we conducted an additional round of SNP calling using bam files from the initial *M. vitellinus*, *candei*, and hybrid sequencing as well as bam files from the subsequent *M. manacus* and *M. aurantiacus* sequencing as inputs for GATK HaplotypeCaller and CombineGVCFs and then filtered using the following terms: "QD < 2.0 || FS > 60.0 || SOR > 3.0 || MQ < 40.0 || ReadPosRankSum < −3.0 || ReadPosRankSum > 3.0 || BaseQRankSum < −3.0 || BaseQRankSum > 3.0 || MQRankSum < −3.0 || MQRankSum > 3.0" and "DP < 4.0 || GQ < 3.0." Last, we filtered out indels and any sites missing in more than 10 of 15 individuals.

ABBA-BABA statistics require a four-species tree, and the calculation of the f_d statistic makes the assumption that, in the tree structure (((P1,P2),P3,)P4), gene flow is directional from P3 to P2 (*43*). Gene flow in the opposite direction will still result in elevated f_d, but the signal will be reduced. We used the genomics_general package (https://github.com/simonhmartin/genomics_general) to calculate f_d across the genome in 10-kb windows (*43*) with trans-Andean *M. manacus* as P1, *M. vitellinus* as P2, *M. aurantiacus* as P3, and cis-Andean *M. manacus* as P4. We changed values of f_d to zero in windows where *D* was negative, where f_d was negative, or where f_d was greater than one, as recommended by the author. Removing windows with fewer than 100 sites used to calculate f_d is recommended by the author to reduce stochastic variation in f_d (fig. S38A), but this cutoff was not feasible for our dataset (fig. S38B). Instead, we used a 50-site cutoff.

For a finer-scale view of introgression evidence in the *BCO2* region, we calculated f_d on chromosome 24 using 2-kb windows and a 10-site minimum cutoff. Using the all-species VCF file described above, we also made trees in 100-bp windows across the chromosome. For this analysis, we subset the main VCF into a window and then obtained the consensus sequence for each of four species (*M. vitellinus*, trans-Andean *M. manacus*, parental *M. candei*, and *M. aurantiacus*) using bcftools v1.18 (*114*), aligned the sequences with Mafft v7.520 (*112*), and built a tree using fasttree v2.1.11 (*115*). Next, we identified all trees in which *M. aurantiacus* and *M. vitellinus* were sister to one another and calculated the frequency of such trees in consecutive bins of 20 and 100 windows across the chromosome, corresponding to 2- and 10-kb bin sizes, respectively.

Feather water shedding in *Manacus*

The waterproofing of a bird's feathers is determined by two forces: water repellency and water penetration resistance (*34*). Water repellency is described as the ability for a feather to cause water to bead and shed from its surface, and water penetration resistance can be defined as the force required to push water through the barbs of overlapping feathers (*34*). These forces are in partial physical opposition to each other, as they are both determined by the diameter of a feather's barbs and the spacing between adjacent barbs (*34*).

Mathematical estimations of water repellency and water penetration resistance have been developed on the basis of the similarity of morphology of feather structure to adjacent and overlapping cylindrical surfaces (*34*). These estimates have been applied to multiple bird species that inhabit aquatic and arboreal habitats (*35*, *116*). Terrestrial and arboreal birds are believed to benefit the most from maximizing water repellency, while aquatic birds benefit most from penetration resistance (*86*, *116*). Here, we use these estimates to examine the collar feathers of the four species in the genus *Manacus* (*M. manacus*, *M. candei*, *M. vitellinus*, and *M. aurantiacus*) and the *M. candei* x *M. vitellinus* hybrids that attained *vitellinus* plumage coloration through genetic introgression. We compared feathers from each species and the hybrids to look for differences in feather structure that could lead to fitness-related consequences in terms of waterproofing ability. We used light microscopy, photographical measurement, and wettability modeling to estimate the ability of feathers to repel water and resist water penetration.

For microstructural analyses, we used the same collar feathers from the color analyses described above. From the collar feathers, we sampled the most intact feather from each of the six individuals per taxon. The feathers chosen were not used in any color analysis beyond light microscopy—they were not subjected to HPLC or spectroscopy before our measurement for this analysis. Each feather was examined under reflected light on a glass calibration slide with an etched scale accurate to 0.1 mm. Feathers were placed on this scale, and pictures were taken using an AmScope Microscope Digital Camera at a magnification of ×40. Photographs were imported into FIJI software, and morphological measurements were recorded using the calibration slide scale as reference. We recorded feather measurements in the middle of the feather to avoid any fraying of the feather edges influencing the data according to the recommendation in (*34*). We recorded two main metrics in accordance with the methods of (*34*, *35*): feather barb width and the spacing between feather barbs. We also recorded barb length from the base of the barb to the distal tip. From each feather, we recorded these measurements using five barbs and, therefore, retained feather ID in all statistical models to

control for pseudoreplication and non-independence of barb measurements within each feather.

We calculated water repellency using Eq. 1 below, as described in (*34*)

$$(R + D) / R \quad (1)$$

where R is equal to the radius of each barb and D is equal to half the distance between adjacent barbs. Lower values of the repellency estimate indicate reduced water repellency and higher values represent better water repellency. To estimate water penetration resistance, we used Eq. 2 below, also as described in (*34*)

$$P = \frac{\gamma}{R'} \quad (2)$$

where P is the pressure required to force water between feather barbs in grams per square centimeter, γ is the surface tension of water, and R' is the principal radius of curvature of a feather barb, calculated using Eq. 3 below

$$R' = \cos\theta + \sqrt{\left\{\frac{R + D}{R}\right\}^2 - \sin^2\theta} \quad (3)$$

where θ is the contact of angle of water with the feather surface. As in Rijke *et al.* (*34*, *35*), we set γ to be equal to the surface tension of water at 20°C (72.86 dynes/cm) and θ to be equal to 90°.

We calculated differences among taxa in barb width, barb spacing, barb length, water repellency $[(R + D)/R]$, and water penetration resistance using linear mixed effects models in R using the lme4 package (*117*) and corrected for multiple comparisons using the emmeans package v.1.8.5 (*90*). In this model, we used taxon as a fixed effect and feather ID as a random effect to control for the fact that five barb measurements came from each feather. We plotted our results using the cowplot v.1.1.1 (*92*), ggpubr v.0.6.0 (*91*), and patchwork v1.1.2 (*118*) packages. From each model analysis, we report the estimated effect size (β: the difference between groups), the SE, and the confidence interval around the estimated effect size and the associated P value in table S4.

Supplementary Materials

The PDF file includes:

Supplementary Text
Figs. S1 to S40
Tables S1 to S16
Legend for movie S1
Legends for data S1 and S2
References

Other Supplementary Material for this manuscript includes the following:

Movie S1
Data S1 and S2

REFERENCES AND NOTES

1. M. J. Ryan, *A Taste for the Beautiful: The Evolution of Attraction* (Princeton Univ. Press, 2018).
2. M. Andersson, *Sexual Selection* (Princeton Univ. Press, 1994).
3. W. J. Swanson, V. D. Vacquier, The rapid evolution of reproductive proteins. *Nat. Rev. Genet.* **3**, 137–144 (2002).
4. G. S. Wilkinson, F. Breden, J. E. Mank, M. G. Ritchie, A. D. Higginson, J. Radwan, J. Jaquiery, W. Salzburger, E. Arriero, S. M. Barribeau, P. C. Phillips, S. C. P. Renn, L. Rowe, The locus of sexual selection: Moving sexual selection studies into the post-genomics era. *J. Evol. Biol.* **28**, 739–755 (2015).
5. L. Rowe, H. D. Rundle, The alignment of natural and sexual selection. *Annu. Rev. Ecol. Evol. Syst.* **52**, 499–517 (2021).
6. S. A. Taylor, E. L. Larson, Insights from genomes into the evolutionary importance and prevalence of hybridization in nature. *Nat. Ecol. Evol.* **3**, 170–177 (2019).
7. D. A. Marques, J. I. Meier, O. Seehausen, A combinatorial view on speciation and adaptive radiation. *Trends Ecol. Evol.* **34**, 531–544 (2019).
8. B. M. Moran, C. Payne, Q. Langdon, D. L. Powell, Y. Brandvain, M. Schumer, The genomic consequences of hybridization. *eLife* **10**, e69016 (2021).
9. D. Berner, W. Salzburger, The genomics of organismal diversification illuminated by adaptive radiations. *Trends Genet.* **31**, 491–499 (2015).
10. K. J. Liu, E. Steinberg, A. Yozzo, Y. Song, M. H. Kohn, L. Nakhleh, Interspecific introgressive origin of genomic diversity in the house mouse. *Proc. Natl. Acad. Sci. U.S.A.* **112**, 196–201 (2015).
11. A. Suarez-Gonzalez, C. A. Hefer, C. Christe, O. Corea, C. Lexer, Q. C. B. Cronk, C. J. Douglas, Genomic and functional approaches reveal a case of adaptive introgression from *Populus balsamifera* (balsam poplar) in *P. trichocarpa* (black cottonwood). *Mol. Ecol.* **25**, 2427–2442 (2016).
12. M. R. Jones, L. S. Mills, P. C. Alves, C. M. Callahan, J. M. Alves, D. J. R. Lafferty, F. M. Jiggins, J. D. Jensen, J. Melo-Ferreira, J. M. Good, Adaptive introgression underlies polymorphic seasonal camouflage in snowshoe hares. *Science* **360**, 1355–1358 (2018).
13. T. J. Parsons, S. L. Olson, M. J. Braun, Unidirectional spread of secondary sexual plumage traits across an avian hybrid zone. *Science* **260**, 1643–1646 (1993).
14. D. T. Baldassarre, T. A. White, J. Karubian, M. S. Webster, Genomic and morphological analysis of a semipermeable avian hybrid zone suggests asymmetrical introgression of a sexual signal. *Evolution* **68**, 2644–2657 (2014).
15. G. M. While, S. Michaelides, R. J. P. Heathcote, H. E. A. MacGregor, N. Zajac, J. Beninde, P. Carazo, G. Pérez i de Lanuza, R. Sacchi, M. A. L. Zuffi, T. Horváthová, B. Fresnillo, U. Schulte, M. Veith, A. Hochkirch, T. Uller, Sexual selection drives asymmetric introgression in wall lizards. *Ecol. Lett.* **18**, 1366–1375 (2015).
16. S. E. Lipshutz, J. I. Meier, G. E. Derryberry, M. J. Miller, O. Seehausen, E. P. Derryberry, Differential introgression of a female competitive trait in a hybrid zone between sex-role reversed species. *Evolution* **73**, 188–201 (2019).
17. O. Seehausen, Y. Terai, I. S. Magalhaes, K. L. Carleton, H. D. J. Mrosso, R. Miyagi, I. van der Sluijs, M. V. Schneider, M. E. Maan, H. Tachida, H. Imai, N. Okada, Speciation through sensory drive in cichlid fish. *Nature* **455**, 620–626 (2008).
18. N. Seddon, C. A. Botero, J. A. Tobias, P. O. Dunn, H. E. A. MacGregor, D. R. Rubenstein, J. A. C. Uy, J. T. Weir, L. A. Whittingham, R. J. Safran, Sexual selection accelerates signal evolution during speciation in birds. *Proc. R. Soc. B Biol. Sci.* **280**, 20131065 (2013).
19. M. J. Ryan, M. E. Cummings, Perceptual biases and mate choice. *Annu. Rev. Ecol. Evol. Syst.* **44**, 437–459 (2013).
20. G. E. Hill, Plumage coloration is a sexually selected indicator of male quality. *Nature* **350**, 337–339 (1991).
21. J. D. Ligon, *The Evolution of Avian Breeding Systems* (Oxford Univ. Press, 1999).
22. M. Â. Marini, S. J. Hackett, A multifaceted approach to the characterization of an intergeneric hybrid manakin (Pipridae) from Brazil. *Auk* **119**, 1114–1120 (2002).
23. R. T. Brumfield, R. W. Jernigan, D. B. McDonald, M. J. Braun, Evolutionary implications of divergent clines in an avian (*Manacus*: Aves) hybrid zone. *Evolution* **55**, 2070–2087 (2001).
24. A. O. Barrera-Guzmán, A. Aleixo, M. D. Shawkey, J. T. Weir, Hybrid speciation leads to novel male secondary sexual ornamentation of an Amazonian bird. *Proc. Natl. Acad. Sci. U.S.A.* **115**, E218–E225 (2018).
25. A. E. Moncrieff, B. C. Faircloth, R. T. Brumfield, Systematics of *Lepidothrix* manakins (Aves: Passeriformes: Pipridae) using RADcap markers. *Mol. Phylogenet. Evol.* **173**, 107525 (2022).
26. W. R. Lindsay, J. T. Houck, C. E. Giuliano, L. B. Day, Acrobatic courtship display coevolves with brain size in manakins (Pipridae). *Brain Behav. Evol.* **85**, 29–36 (2015).
27. A. C. Stein, J. A. C. Uy, Plumage brightness predicts male mating success in the lekking golden-collared manakin, *Manacus vitellinus*. *Behav. Ecol.* **17**, 41–47 (2006).
28. A. C. Stein, J. A. C. Uy, Unidirectional introgression of a sexually selected trait across an avian hybrid zone: A role for female choice? *Evolution* **60**, 1476–1485 (2006).
29. K. M. Long, A. G. Rivera-Colón, K. F. P. Bennett, J. M. Catchen, M. J. Braun, J. D. Brawn, Ongoing introgression of a secondary sexual plumage trait in a stable avian hybrid zone. *Evolution* **78**, 1539–1553 (2024).
30. D. B. McDonald, R. P. Clay, R. T. Brumfield, M. J. Braun, Sexual selection on plumage and behavior in an avian hybrid zone: Experimental tests of male-male interactions. *Evolution* **55**, 1443–1451 (2001).
31. J. Barske, M. J. Fuxjager, C. Ciofi, C. Natali, B. A. Schlinger, T. Billo, L. Fusani, Beyond plumage: Acrobatic courtship displays show intermediate patterns in manakin hybrids. *Anim. Behav.* **198**, 195–205 (2023).
32. K. F. P. Bennett, H. C. Lim, M. J. Braun, Sexual selection and introgression in avian hybrid zones: Spotlight on *Manacus*. *Integr. Comp. Biol.* **61**, 1291–1309 (2021).
33. R. Maia, H. Gruson, J. A. Endler, T. E. White, pavo 2: New tools for the spectral and spatial analysis of colour in r. *Methods Ecol. Evol.* **10**, 1097–1107 (2019).

34. A. M. Rijke, Wettability and phylogenetic development of feather structure in water birds. *J. Exp. Biol.* **52**, 469–479 (1970).
35. A. M. Rijke, W. A. Jesser, S. W. Evans, H. Bouwman, Water repellency and feather structure of the Blue Swallow *Hirundo atrocaerulea*. *Ostrich* **71**, 143–145 (2000).
36. T. L. Parchman, Z. Gompert, M. J. Braun, R. T. Brumfield, D. B. McDonald, J. A. C. Uy, G. Zhang, E. D. Jarvis, B. A. Schlinger, C. A. Buerkle, The genomic consequences of adaptive divergence and reproductive isolation between species of manakins. *Mol. Ecol.* **22**, 3304–3317 (2013).
37. M. A. K. Widjaja-Adhi, M. Golczak, The molecular aspects of absorption and metabolism of carotenoids and retinoids in vertebrates. *Biochim. Biophys. Acta Mol. Cell Biol. Lipids* **1865**, 158571 (2020).
38. H. Bellil, F. Ghieh, E. Hermel, B. Mandon-Pepin, F. Vialard, Human testis-expressed (TEX) genes: A review focused on spermatogenesis and male fertility. *Basic Clin. Androl.* **31**, 9 (2021).
39. B. Thöny, G. Auerbach, N. Blau, Tetrahydrobiopterin biosynthesis, regeneration and functions. *Biochem J* **347**, 1–16 (2000).
40. T. E. Cruickshank, M. W. Hahn, Reanalysis suggests that genomic islands of speciation are due to reduced diversity, not reduced gene flow. *Mol. Ecol.* **23**, 3133–3157 (2014).
41. R. Burri, Interpreting differentiation landscapes in the light of long-term linked selection. *Evol. Lett.* **1**, 118–131 (2017).
42. M. Nei, *Molecular Evolutionary Genetics* (Columbia Univ. Press, 1987).
43. S. H. Martin, J. W. Davey, C. D. Jiggins, Evaluating the use of ABBA–BABA statistics to locate introgressed loci. *Mol. Biol. Evol.* **32**, 244–257 (2015).
44. J. L. Feder, X. Xie, J. Rull, S. Velez, A. Forbes, B. Leung, H. Dambroski, K. E. Filchak, M. Aluja, Mayr, Dobzhansky, and Bush and the complexities of sympatric speciation in *Rhagoletis*. *Proc. Natl. Acad. Sci. U.S.A.* **102**, 6573–6580 (2005).
45. J. Strychalski, P. Brym, U. Czarnik, A. Gugołek, A novel AAT-deletion mutation in the coding sequence of the *BCO2* gene in yellow-fat rabbits. *J. Appl. Genetics* **56**, 535–537 (2015).
46. D. P. L. Toews, S. A. Taylor, R. Vallender, A. Brelsford, B. G. Butcher, P. W. Messer, I. J. Lovette, Plumage genes and little else distinguish the genomes of hybridizing warblers. *Curr. Biol.* **26**, 2313–2318 (2016).
47. M. A. Gazda, P. M. Araújo, R. J. Lopes, M. B. Toomey, P. Andrade, S. Afonso, C. Marques, L. Nunes, P. Pereira, S. Trigo, G. E. Hill, J. C. Corbo, M. Carneiro, A genetic mechanism for sexual dichromatism in birds. *Science* **368**, 1270–1274 (2020).
48. J. Eriksson, G. Larson, U. Gunnarsson, B. Bed'hom, M. Tixier-Boichard, L. Strömstedt, D. Wright, A. Jungerius, A. Vereijken, E. Randi, P. Jensen, L. Andersson, Identification of the yellow skin gene reveals a hybrid origin of the domestic chicken. *PLOS Genet.* **4**, e1000010 (2008).
49. M. D. Baiz, A. W. Wood, A. Brelsford, I. J. Lovette, D. P. L. Toews, Pigmentation genes show evidence of repeated divergence and multiple bouts of introgression in *Setophaga* warblers. *Curr. Biol.* **31**, 643–649.e3 (2021).
50. P. Andrade, C. Pinho, G. Pérez i de Lanuza, S. Afonso, J. Brejcha, C.-J. Rubin, O. Wallerman, P. Pereira, S. J. Sabatino, A. Bellati, D. Pellitteri-Rosa, Z. Bosakova, I. Bunikis, M. A. Carretero, N. Feiner, P. Marsik, F. Paupério, D. Salvi, L. Soler, G. M. While, T. Uller, E. Font, L. Andersson, M. Carneiro, Regulatory changes in pterin and carotenoid genes underlie balanced color polymorphisms in the wall lizard. *Proc. Natl. Acad. Sci. U.S.A.* **116**, 5633–5642 (2019).
51. S. J. Lehnert, K. A. Christensen, W. E. Vandersteen, D. Sakhrani, T. E. Pitcher, J. W. Heath, B. F. Koop, D. D. Heath, R. H. Devlin, Carotenoid pigmentation in salmon: Variation in expression at *BCO2*-l locus controls a key fitness trait affecting red coloration. *Proc. R. Soc. B Biol. Sci.* **286**, 20191588 (2019).
52. E. D. Enbody, C. G. Sprehn, A. Abzhanov, H. Bi, M. P. Dobreva, O. G. Osborne, C.-J. Rubin, P. R. Grant, B. R. Grant, L. Andersson, A multispecies *BCO2* beak color polymorphism in the Darwin's finch radiation. *Curr. Biol.* **31**, 5597–5604.e7 (2021).
53. C. R. Linnen, E. P. Kingsley, J. D. Jensen, H. E. Hoekstra, On the origin and spread of an adaptive allele in deer mice. *Science* **325**, 1095–1098 (2009).
54. M. Abolins-Abols, E. Kornobis, P. Ribeca, K. Wakamatsu, M. P. Peterson, E. D. Ketterson, B. Milá, Differential gene regulation underlies variation in melanic plumage coloration in the dark-eyed junco (*Junco hyemalis*). *Mol. Ecol.* **27**, 4501–4515 (2018).
55. Y.-R. Jin, J. K. Yoon, The R-spondin family of proteins: Emerging regulators of WNT signaling. *Int. J. Biochem. Cell Biol.* **44**, 2278–2287 (2012).
56. A. I. Vickrey, R. Bruders, Z. Kronenberg, E. Mackey, R. J. Bohlender, E. T. Maclary, R. Maynez, E. J. Osborne, K. P. Johnson, C. D. Huff, M. Yandell, M. D. Shapiro, Introgression of regulatory alleles and a missense coding mutation drive plumage pattern diversity in the rock pigeon. *elife* **7**, e34803 (2018).
57. E. Cadieu, M. W. Neff, P. Quignon, K. Walsh, K. Chase, H. G. Parker, B. M. VonHoldt, A. Rhue, A. Boyko, A. Byers, A. Wong, D. S. Mosher, A. G. Elkahloun, T. C. Spady, C. André, K. G. Lark, M. Cargill, C. D. Bustamante, R. K. Wayne, E. A. Ostrander, Coat variation in the domestic dog is governed by variants in three genes. *Science* **326**, 150–153 (2009).
58. N. Chaves, Orange-collared Manakin (*Manacus aurantiacus*), version 1.0, *Birds of the World* (2020). https://birdsoftheworld.org/bow/species/orcman1/cur/introduction.
59. N. D. Sly, Golden-collared Manakin (*Manacus vitellinus*), version 2.0, *Birds of the World* (2023). https://birdsoftheworld.org/bow/species/gocman1/cur/introduction.
60. S. Andersson, M. Prager, "Quantifying Colors" in *Bird Coloration*, G. Hill, K. McGraw, Eds. (Harvard Univ. Press, 2006), pp. 81.
61. D. A. Gray, Carotenoids and Sexual Dichromatism in North American Passerine Birds. *Am. Nat.* **148**, 453–480 (1996).
62. S. L. Olson, Specializations of some carotenoid-bearing feathers. *Condor* **72**, 424–430 (1970).
63. A. L. Potticary, E. S. Morrison, A. V. Badyaev, Turning induced plasticity into refined adaptations during range expansion. *Nat. Commun.* **11**, 3254 (2020).
64. D. M. Troy, A. H. Brush, Pigments and feather structure of the redpolls, *Carduelis flammea* and *C. hornemanni*. *Condor* **85**, 443–446 (1983).
65. D. E. McCoy, A. J. Shultz, C. Vidoudez, E. van der Heide, J. E. Dall, S. A. Trauger, D. Haig, Microstructures amplify carotenoid plumage signals in tanagers. *Sci. Rep.* **11**, 8582 (2021).
66. M. A. Gazda, M. B. Toomey, P. M. Araújo, R. J. Lopes, S. Afonso, C. A. Myers, K. Serres, P. D. Kiser, G. E. Hill, J. C. Corbo, M. Carneiro, Genetic basis of de novo appearance of carotenoid ornamentation in bare parts of canaries. *Mol. Biol. Evol.* **37**, 1317–1328 (2020).
67. J. B. Pease, R. J. Driver, D. A. de la Cerda, L. B. Day, W. R. Lindsay, B. A. Schlinger, E. R. Schuppe, C. N. Balakrishnan, M. J. Fuxjager, Layered evolution of gene expression in "superfast" muscles for courtship. *Proc. Natl. Acad. Sci. U.S.A.* **119**, e2119671119 (2022).
68. W. P. Maddison, Gene Trees in Species Trees. *Syst. Biol.* **46**, 523–536 (1997).
69. R. N. Leite, R. T. Kimball, E. L. Braun, E. P. Derryberry, P. A. Hosner, G. E. Derryberry, M. Anciães, J. S. McKay, A. Aleixo, C. C. Ribas, R. T. Brumfield, J. Cracraft, Phylogenomics of manakins (Aves: Pipridae) using alternative locus filtering strategies based on informativeness. *Mol. Phylogenet. Evol.* **155**, 107013 (2021).
70. D. B. McDonald, T. L. Parchman, M. R. Bower, W. A. Hubert, F. J. Rahel, An introduced and a native vertebrate hybridize to form a genetic bridge to a second native species. *Proc. Natl. Acad. Sci. U.S.A.* **105**, 10837–10842 (2008).
71. P. J. Wilson, L. Y. Rutledge, T. J. Wheeldon, B. R. Patterson, B. N. White, Y-chromosome evidence supports widespread signatures of three-species *Canis* hybridization in eastern North America. *Ecol. Evol.* **2**, 2325–2332 (2012).
72. M. L. Haines, J. Melville, J. Sumner, N. Clemann, D. G. Chapple, D. Stuart-Fox, Geographic variation in hybridization and ecological differentiation between three syntopic, morphologically similar species of montane lizards. *Mol. Ecol.* **25**, 2887–2903 (2016).
73. Q. K. Langdon, D. Peris, E. P. Baker, D. A. Opulente, H.-V. Nguyen, U. Bond, P. Gonçalves, J. P. Sampaio, D. Libkind, C. T. Hittinger, Fermentation innovation through complex hybridization of wild and domesticated yeasts. *Nat. Ecol. Evol.* **3**, 1576–1586 (2019).
74. P. R. Grant, B. R. Grant, Triad hybridization via a conduit species. *Proc. Natl. Acad. Sci. U.S.A.* **117**, 7888–7896 (2020).
75. L. Natola, S. S. Seneviratne, D. Irwin, Population genomics of an emergent tri-species hybrid zone. *Mol. Ecol.* **31**, 5356–5367 (2022).
76. M. S. Ferreira, T. J. Thurman, M. R. Jones, L. Farelo, A. V. Kumar, S. M. E. Mortimer, J. R. Demboski, L. S. Mills, P. C. Alves, J. Melo-Ferreira, J. M. Good, The evolution of white-tailed jackrabbit camouflage in response to past and future seasonal climates. *Science* **379**, 1238–1242 (2023).
77. J. I. Meier, M. D. McGee, D. A. Marques, S. Mwaiko, M. Kishe, S. Wandera, D. Neumann, H. Mrosso, L. J. Chapman, C. A. Chapman, L. Kaufman, A. Taabu-Munyaho, C. E. Wagner, R. Bruggmann, L. Excoffier, O. Seehausen, Cycles of fusion and fission enabled rapid parallel adaptive radiations in African cichlids. *Science* **381**, eade2833 (2023).
78. N. B. Edelman, P. B. Frandsen, M. Miyagi, B. Clavijo, J. Davey, R. B. Dikow, G. García-Accinelli, S. M. Van Belleghem, N. Patterson, D. E. Neafsey, R. Challis, S. Kumar, G. R. P. Moreira, C. Salazar, M. Chouteau, B. A. Counterman, R. Papa, M. Blaxter, R. D. Reed, K. K. Dasmahapatra, M. Kronforst, M. Joron, C. D. Jiggins, W. O. McMillan, F. Di Palma, A. J. Blumberg, J. Wakeley, D. Jaffe, J. Mallet, Genomic architecture and introgression shape a butterfly radiation. *Science* **366**, 594–599 (2019).
79. E. J. Beckman, P. M. Benham, Z. A. Cheviron, C. C. Witt, Detecting introgression despite phylogenetic uncertainty: The case of the South American siskins. *Mol. Ecol.* **27**, 4350–4367 (2018).
80. A.-L. Ducrest, L. Keller, A. Roulin, Pleiotropy in the melanocortin system, coloration and behavioural syndromes. *Trends Ecol. Evol.* **23**, 502–510 (2008).
81. R. J. Weaver, E. S. A. Santos, A. M. Tucker, A. E. Wilson, G. E. Hill, Carotenoid metabolism strengthens the link between feather coloration and individual quality. *Nat. Commun.* **9**, 73 (2018).
82. R. T. Brumfield, M. J. Braun, Phylogenetic relationships in bearded manakins (Pipridae: *Manacus*) indicate that male plumage color is a misleading taxonomic marker. *Condor* **103**, 248–258 (2001).
83. J. A. C. Uy, A. C. Stein, Variable visual habitats may influence the spread of colourful plumage across an avian hybrid zone. *J. Evol. Biol.* **20**, 1847–1858 (2007).
84. E. H. DuVal, C. L. Fitzpatrick, E. A. Hobson, M. R. Servedio, Inferred Attractiveness: A generalized mechanism for sexual selection that can maintain variation in traits and preferences over time. *PLOS Biol.* **21**, e3002269 (2023).

85. W. A. Boyle, E. H. Shogren, J. D. Brawn, Hygric Niches for Tropical Endotherms. *Trends Ecol. Evol.* **35**, 938–952 (2020).
86. R. J. Kennedy, Direct effects of rain on birds: A review. *British Birds* **63**, 401–414 (1970).
87. S. E. Fick, R. J. Hijmans, WorldClim 2: New 1-km spatial resolution climate surfaces for global land areas. *Int. J. Climatol.* **37**, 4302–4315 (2017).
88. F. M. S. Muzio, M. A. Rubega, What do we really know about the water repellency of feathers? *J. Avian Biol.* 10.1111/jav.03259 , (2024).
89. R Core Team, R: A language and environment for statistical computing, R Foundation for Statistical Computing (2024); https://R-project.org/.
90. R. Lenth, emmeans: Estimated Marginal Means, aka Least-Squares Means, (2020); https://cran.r-project.org/package=emmeans.
91. A. Kassambara, ggpubr: "ggplot2" based publication ready plots, (2019); https://cran.r-project.org/package=ggpubr.
92. C. O. Wilke, cowplot: Streamlined Plot Theme and Plot Annotations for "ggplot2," CRAN Repos (2016); https://cran.r-project.org/package=cowplot.
93. B. Langmead, S. L. Salzberg, Fast gapped-read alignment with Bowtie 2. *Nat. Methods.* **9**, 357–359 (2012).
94. H. Li, B. Handsaker, A. Wysoker, T. Fennell, J. Ruan, N. Homer, G. Marth, G. Abecasis, R. Durbin; 1000 Genome Project Data Processing Subgroup, The sequence alignment/map format and SAMtools. *Bioinformatics* **25**, 2078–2079 (2009).
95. A. V. Zimin, G. Marçais, D. Puiu, M. Roberts, S. L. Salzberg, J. A. Yorke, The MaSuRCA genome assembler. *Bioinformatics* **29**, 2669–2677 (2013).
96. G. A. Van der Auwera, B. D. O'Connor, *Genomics in the Cloud: Using Docker, GATK, and WDL in Terra* (O'Reilly Media, 2020).
97. M. Alonge, S. Soyk, S. Ramakrishnan, X. Wang, S. Goodwin, F. J. Sedlazeck, Z. B. Lippman, M. C. Schatz, RaGOO: Fast and accurate reference-guided scaffolding of draft genomes. *Genome Biol.* **20**, 224 (2019).
98. D. Bryant, V. Moulton, Neighbor-net: An agglomerative method for the construction of phylogenetic networks. *Mol. Biol. Evol.* **21**, 255–265 (2004).
99. D. H. Huson, D. Bryant, Application of phylogenetic networks in evolutionary studies. *Mol. Biol. Evol.* **23**, 254–267 (2006).
100. H. E. Lischer, L. Excoffier, PGDSpider: An automated data conversion tool for connecting population genetics and genomics programs. *Bioinformatics* **28**, 298–299 (2012).
101. T. S. Korneliussen, A. Albrechtsen, R. Nielsen, ANGSD: Analysis of next generation sequencing data. *BMC Bioinformatics* **15**, 356 (2014).
102. M. Fumagalli, F. G. Vieira, T. S. Korneliussen, T. Linderoth, E. Huerta-Sánchez, A. Albrechtsen, R. Nielsen, Quantifying population genetic differentiation from next-generation sequencing data. *Genetics* **195**, 979–992 (2013).
103. A. J. Coffman, P. H. Hsieh, S. Gravel, R. N. Gutenkunst, Computationally efficient composite likelihood statistics for demographic inference. *Mol. Biol. Evol.* **33**, 591–593 (2016).
104. T. R. Booker, S. Yeaman, M. C. Whitlock, Variation in recombination rate affects detection of outliers in genome scans under neutrality. *Mol. Ecol.* **29**, 4274–4279 (2020).
105. A. Zeileis, G. Grothendieck, J. A. Ryan, J. M. Ulrich, F. Andrews, zoo: S3 Infrastructure for Regular and Irregular Time Series (Z's Ordered Observations), version 1.8-12, (2023); https://cran.r-project.org/web/packages/zoo/index.html.
106. H. Mi, A. Muruganujan, D. Ebert, X. Huang, P. D. Thomas, PANTHER version 14: More genomes, a new PANTHER GO-slim and improvements in enrichment analysis tools. *Nucleic Acids Res.* **47**, D419–D426 (2019).
107. H. Mi, P. Thomas, Protein networks and pathway analysis. *Methods Mol. Biol.* **563**, 123–140 (2009).
108. A. Dobin, C. A. Davis, F. Schlesinger, J. Drenkow, C. Zaleski, S. Jha, P. Batut, M. Chaisson, T. R. Gingeras, STAR: Ultrafast universal RNA-seq aligner. *Bioinformatics* **29**, 15–21 (2013).
109. Y. Liao, G. K. Smyth, W. Shi, featureCounts: An efficient general purpose program for assigning sequence reads to genomic features. *Bioinformatics* **30**, 923–930 (2014).
110. H. Li, Aligning sequence reads, clone sequences and assembly contigs with BWA-MEM. arXiv:1303.3997 [q-bio.GN] (2013).
111. P. Danecek, A. Auton, G. Abecasis, C. A. Albers, E. Banks, M. A. DePristo, R. E. Handsaker, G. Lunter, G. T. Marth, S. T. Sherry, G. McVean, R. Durbin; 1000 Genomes Project Analysis Group, The variant call format and VCFtools. *Bioinformatics* **27**, 2156–2158 (2011).
112. K. Katoh, D. M. Standley, MAFFT multiple sequence alignment software version 7: Improvements in performance and usability. *Mol. Biol. Evol.* **30**, 772–780 (2013).
113. B. Q. Minh, H. A. Schmidt, O. Chernomor, D. Schrempf, M. D. Woodhams, A. von Haeseler, R. Lanfear, IQ-TREE 2: New models and efficient methods for phylogenetic inference in the genomic era. *Mol. Biol. Evol.* **37**, 1530–1534 (2020).
114. P. Danecek, J. K. Bonfield, J. Liddle, J. Marshall, V. Ohan, M. O. Pollard, A. Whitwham, T. Keane, S. A. McCarthy, R. M. Davies, H. Li, Twelve years of SAMtools and BCFtools. *GigaScience* **10**, giab008 (2021).
115. M. N. Price, P. S. Dehal, A. P. Arkin, FastTree 2—Approximately maximum-likelihood trees for large alignments. *PLOS ONE* **5**, e9490 (2010).
116. A. M. Rijke, W. A. Jesser, The water penetration and repellency of feathers revisited. *The Condor* **113**, 245–254 (2011).
117. D. Bates, M. Mächler, B. Bolker, S. Walker, Fitting linear mixed-effects models using lme4. *J. Stat. Softw.* **67**, 1–48 (2015).
118. T. L. Pedersen, patchwork: The Composer of Plots, version 1.1.2 (2022); https://cran.r-project.org/web/packages/patchwork/index.html.
119. J. Haffer, Speciation in Colombian forest birds west of the Andes. *Am. Mus. Novit.* **2294**, 58 (1967).
120. M. G. Harvey, G. A. Bravo, S. Claramunt, A. M. Cuervo, G. E. Derryberry, J. Battilana, G. F. Seeholzer, J. S. McKay, B. C. O'Meara, B. C. Faircloth, S. V. Edwards, J. Pérez-Emán, R. G. Moyle, F. H. Sheldon, A. Aleixo, B. T. Smith, R. T. Chesser, L. F. Silveira, J. Cracraft, R. T. Brumfield, E. P. Derryberry, The evolution of a tropical biodiversity hotspot. *Science* **370**, 1343–1348 (2020).
121. K. J. McGraw, J. Hudon, G. E. Hill, R. S. Parker, A simple and inexpensive chemical test for behavioral ecologists to determine the presence of carotenoid pigments in animal tissues. *Behav. Ecol. Sociobiol.* **57**, 391–397 (2005).
122. K. J. McGraw, E. Adkins-Regan, R. S. Parker, Anhydrolutein in the zebra finch: A new, metabolically derived carotenoid in birds. *Comp. Biochem. Physiol. B Biochem. Mol. Biol.* **132**, 811–818 (2002).
123. S. W. Wright, S. W. Jeffrey, R. F. C. Mantoura, C. A. Llewelly, T. Bjornland, D. Repeta, N. Welschmeyer, Improved HPLC method for the analysis of chlorophylls and carotenoids from marine phytoplankton. *Mar. Ecol. Prog. Ser.* **77**, 183–196 (1991).
124. N. H. Barton, Genetic hitchhiking. *Philos. Trans. R. Soc. Lond. B Biol. Sci.* **355**, 1553–1562 (2000).
125. A. S. Y. Lee, P. J. Kranzusch, J. H. D. Cate, eIF3 targets cell-proliferation messenger RNAs for translational activation or repression. *Nature* **522**, 111–114 (2015).
126. S. Wang, S. Rohwer, D. R. de Zwaan, D. P. L. Toews, I. J. Lovette, J. Mackenzie, D. Irwin, Selection on a small genomic region underpins differentiation in multiple color traits between two warbler species. *Evol. Lett.* **4**, 502–515 (2020).
127. F. Liu, M. Visser, D. L. Duffy, P. G. Hysi, L. C. Jacobs, O. Lao, K. Zhong, S. Walsh, L. Chaitanya, A. Wollstein, G. Zhu, G. W. Montgomery, A. K. Henders, M. Mangino, D. Glass, V. Bataille, R. A. Sturm, F. Rivadeneira, A. Hofman, W. F. J. van IJcken, A. G. Uitterlinden, R.-J. T. S. Palstra, T. D. Spector, N. G. Martin, T. E. C. Nijsten, M. Kayser, Genetics of skin color variation in Europeans: Genome-wide association studies with functional follow-up. *Hum Genet* **134**, 823–835 (2015).
128. C.-H. Chang, T.-X. Jiang, C.-M. Lin, L. W. Burrus, C.-M. Chuong, R. Widelitz, Distinct Wnt members regulate the hierarchical morphogenesis of skin regions (spinal tract) and individual feathers. *Mech. Dev.* **121**, 157–171 (2004).
129. R. B. Widelitz, G.-W. Lin, Y.-C. Lai, J. A. Mayer, P.-C. Tang, H.-C. Cheng, T.-X. Jiang, C.-F. Chen, C.-M. Chuong, Morpho-regulation in diverse chicken feather formation: Integrating branching modules and sex hormone-dependent morpho-regulatory modules. *Dev. Growth Differ.* **61**, 124–138 (2019).
130. K. F. Stryjewski, M. D. Sorenson, Mosaic genome evolution in a recent and rapid avian radiation. *Nat. Ecol. Evol.* **1**, 1912–1922 (2017).
131. R. Schiffer, M. Neis, D. Höller, F. Rodríguez, A. Geier, C. Gartung, F. Lammert, A. Dreuw, G. Zwadlo-Klarwasser, H. Merk, F. Jugert, J. M. Baron, Active influx transport is mediated by members of the organic anion transporting polypeptide family in human epidermal keratinocytes. *J. Invest. Dermatol.* **120**, 285–291 (2003).
132. K. Sebastian, S. Detro-Dassen, N. Rinis, D. Fahrenkamp, G. Müller-Newen, H. F. Merk, G. Schmalzing, G. Zwadlo-Klarwasser, J. M. Baron, Characterization of SLCO5A1/OATP5A1, a solute carrier transport protein with non-classical function. *PLOS ONE* **8**, e83257 (2013).
133. J. Graf, R. Hodgson, A. van Daal, Single nucleotide polymorphisms in the MATP gene are associated with normal human pigmentation variation. *Hum. Mutat.* **25**, 278–284 (2005).
134. L. Campagna, M. Repenning, L. F. Silveira, C. S. Fontana, P. L. Tubaro, I. J. Lovette, Repeated divergent selection on pigmentation genes in a rapid finch radiation. *Sci. Adv.* **3**, e1602404 (2017).
135. C. Kiefer, S. Hessel, J. M. Lampert, K. Vogt, M. O. Lederer, D. E. Breithaupt, J. von Lintig, Identification and characterization of a mammalian enzyme catalyzing the asymmetric oxidative cleavage of provitamin A. *J. Biol. Chem.* **276**, 14110–14116 (2001).
136. C. dela Seña, J. Sun, S. Narayanasamy, K. M. Riedl, Y. Yuan, R. W. Curley Jr., S. J. Schwartz, E. H. Harrison, Substrate specificity of purified recombinant chicken β-carotene 9′,10′-oxygenase (BCO2). *J. Biol. Chem.* **291**, 14609–14619 (2016).
137. J. Amengual, G. P. Lobo, M. Golczak, H. N. M. Li, T. Klimova, C. L. Hoppel, A. Wyss, K. Palczewski, J. von Lintig, A mitochondrial enzyme degrades carotenoids and protects against oxidative stress. *FASEB J* **25**, 948–959 (2011).
138. G. P. Lobo, A. Isken, S. Hoff, D. Babino, J. von Lintig, BCDO2 acts as a carotenoid scavenger and gatekeeper for the mitochondrial apoptotic pathway. *Development* **139**, 2966–2977 (2012).
139. S. D. Berry, S. R. Davis, E. M. Beattie, N. L. Thomas, A. K. Burrett, H. E. Ward, A. M. Stanfield, M. Biswas, A. E. Ankersmit-Udy, P. E. Oxley, J. L. Barnett, J. F. Pearson, Y. van der Does, A. H. K. MacGibbon, R. J. Spelman, K. Lehnert, R. G. Snell, Mutation in Bovine β-carotene oxygenase 2 affects milk color. *Genetics* **182**, 923–926 (2009).

140. D. I. Våge, I. A. Boman, A nonsense mutation in the beta-carotene oxygenase 2 (BCO2) gene is tightly associated with accumulation of carotenoids in adipose tissue in sheep (*Ovis aries*). *BMC Genetics* **11**, 10 (2010).
141. C.-M. Chuong, The making of a feather: Homeoproteins, retinoids and adhesion molecules. *BioEssays* **15**, 513–521 (1993).
142. Y. Mishima, Molecular and biological control of melanogenesis through tyrosinase genes and intrinsic and extrinsic regulatory factors. *Pigment Cell Res.* **7**, 376–387 (1994).
143. N. I. Mundy, A window on the genetics of evolution: MC1R and plumage colouration in birds. *Proc. Biol. Sci.* **272**, 1633–1640 (2005).
144. E. M. Wolf Horrell, M. C. Boulanger, J. A. D'Orazio, Melanocortin 1 receptor: Structure, function, and regulation. *Front. Genet.* **7**, 95 (2016).

Acknowledgments: We gratefully acknowledge J. Wilkinson, S. Mount, C. Machado, K. Carleton, H. Fisher, M. Baldwin, J. von Lintig, B. Schlinger, L. Fusani, O. McMillan, E. Bermingham, E. Braun, F. Muzio, and C. Dove for providing valuable discussions and comments on study design and drafts of this paper. Sample collection: S. Olson, J. Blake, R. Brumfield, T. Glenn, and D. McDonald. Field assistance: A. Pineda Sr. and A. Pineda Jr. Specimen access: We thank C. Milensky and C. Huddleston for facilitating access to specimens and samples housed in the Smithsonian National Museum of Natural History Bird Collection and Biorepository, respectively. Permits: We are grateful to the following institutions for providing collecting and access permits: Autoridad Nacional del Ambiente and Autoridad del Canal de Panamá, the Guyana Environmental Protection Agency, and Guyana Ministry of Amerindian Affairs. The following people assisted in permit processing: M. Leone, G. Maggiori, L. Camacho, and J. Mate. Computational resources: Computations of genomic data in this paper were conducted on the Smithsonian High-Performance Cluster (SI/HPC), Smithsonian Institution (https://doi.org/10.25572/SIHPC). We thank R. Dikow for providing technical assistance. **Funding:** This work was supported by Smithsonian Institution Competitive Pell Grant (M.J.B. and H.C.L.); Smithsonian Institution James Bond Fund (M.J.B. and K.F.P.B.); National Museum of Natural History Research Grant (M.J.B. and K.F.P.B.); US Department of Agriculture, National Institute of Food and Agriculture, Hatch Project 1026333 (ILLU-875-984) to K.M.L. and J.D.B.; National Science Foundation grant IOS 1122180 (L.B.D.); National Science Foundation grant IOS 1947472 (M.J.F.); National Science Foundation grant IOS 203774 (G.E.H.); National Science Foundation grant DBI 1457541 (M.J.B. and C.N.B.); University of Maryland Devra Kleiman Fellowship (K.F.P.B.); University of Maryland BISI Dissertation Fellowship (K.F.P.B.); and Smithsonian Biodiversity Genomics Postdoctoral Fellowship (H.C.L.). **Author contributions:** Conceptualization: M.J.B., H.C.L., K.F.P.B., K.M.L., J.D.B., and G.E.H. Data collection: H.C.L., K.F.P.B., N.M.J., M.J.P., K.M.L., L.B.D., W.R.L., and T.J.P. Data analysis: H.C.L., K.F.P.B., K.M.L., M.J.P., N.M.J., J.B.P., S.E.K., P.E.B., and M.J.F. Visualization: K.F.P.B., H.C.L., M.J.P., N.M.J., and K.M.L. Supervision: M.J.B., J.D.B., G.E.H., and C.N.B. Writing—original draft: H.C.L., K.F.P.B., M.J.B., N.M.J., M.J.P., G.E.H., and K.M.L. Writing—review and editing: K.F.P.B., H.C.L., M.J.B., M.J.P., N.M.J., G.E.H., P.E.B., J.B.P., S.E.K., L.B.D., T.J.P., K.M.L., J.D.B., M.J.F., and C.N.B. **Competing interests:** The authors declare that they have no competing interests. **Data and materials availability:** Specimens and genetic resource materials used to generate data for this study are housed at the US NMNH, the Louisiana State University Museum of Natural Science, the Academy of Natural Sciences of Drexel University, and the University of Mississippi. Collection access is governed by museum policies, which may be found at https://naturalhistory.si.edu/research/vertebrate-zoology/birds, https://apa.lsu.edu/mns/collections/ornithology.php, and https://ansp.org/research/. Data and code necessary to reproduce the analyses are available from NCBI (BioProjects: PRJNA1129471, PRJNA893627, and PRJNA321179) and on Dryad. DOI: 10.5061/dryad.jsxksn0hn. All other data needed to evaluate the conclusions in the paper are present in the paper and/or the Supplementary Materials.

Submitted 2 January 2024
Accepted 17 October 2024
Published 20 November 2024
10.1126/sciadv.adn8339